

Journal of Geophysical Research: Oceans

RESEARCH ARTICLE

10.1029/2017JC013503

Key Points:

- The use of geodetic measurements in the new MSS (CNES_CLS15, DTU15) contributes to reduce the omission errors by a factor of 2
- The commission errors represent between 10% (CNES_CLS15) and 20% (DTU15) of the SLA variance for wavelengths shorter than 250 km
- MSS errors on uncharted tracks (e.g., Sentinel-3A) explain 30% of the SLA variance at short wavelengths (i.e., 30–100 km)

Correspondence to:M.-I. Pujol,
mpujol@cls.fr**Citation:**

Pujol, M.-I., Schaeffer, P., Faugère, Y., Raynal, M., Dibarboire, G., & Picot, N. (2018). Gauging the improvement of recent mean sea surface models: A new approach for identifying and quantifying their errors. *Journal of Geophysical Research: Oceans*, 123, 5889–5911. <https://doi.org/10.1029/2017JC013503>

Received 5 OCT 2017

Accepted 7 MAY 2018

Accepted article online 11 MAY 2018

Published online 24 AUG 2018

Gauging the Improvement of Recent Mean Sea Surface Models: A New Approach for Identifying and Quantifying Their Errors

Marie-Isabelle Pujol¹ , Philippe Schaeffer¹, Yannice Faugère¹, Matthias Raynal², Gerald Dibarboire³, and Nicolas Picot⁴ 

¹Collecte Localisation Satellites, Environmental Monitoring Division, Toulouse, France, ²Collecte Localisation Satellites, Remote Sensing Division, Toulouse, France, ³Centre National Etudes Spatiales, Direction du Numérique de l'Exploitation et des Opérations, Toulouse, France, ⁴Centre National Etudes Spatiales, Direction des Systèmes Orbitaux, Toulouse, France

Abstract This paper presents an assessment and comparison of recent mean sea surface (MSS) models. Using a new approach and independent altimeter data sets, we quantify the major improvement of the CNES_CLS15 and the DTU15 models. We observe a reduction in the amplitude of omission errors thanks to the use of new geodetic altimeter data sets (i.e., Cryosat-2 and Jason-1 geodetic): they are reduced by a factor of 2 compared with previous generations (CNES_CLS11). We also quantify commission errors resulting from the leakage of residual ocean variability and altimeter noise into the MSS models. For wavelengths shorter than 250 km, the error is of the order of 1–2 cm², i.e., ~10% to 20% of the sea level anomaly (SLA) variance. The global error of both 2015 models has similar orders of magnitude and spectral power densities, although the commission errors of the CNES_CLS15 model are about half as large as those of the DTU15 model. Its absolute error is also slightly smaller than for the DTU15 model in coastal regions and at high latitudes. Conversely, the DTU15 model produces smaller omission errors, especially in the open ocean over strong bathymetric features. More importantly, the MSS errors still have a substantial impact on altimetry products for wavelengths ranging from 30 to 100 km: the error explains ~30% of the global SLA variance, and the error can be 2.5 times higher on uncharted ground tracks (e.g., Sentinel-3) over rugged bathymetry.

1. Introduction

Satellite radar altimetry provides a one-dimensional measurement of ocean surface topography along the satellite's ground track. Escudier et al. (2018) or Le Traon et al. (2014) specify how reference surfaces such as mean sea surface (MSS) are necessary to transform Level 2 ocean topography products into more convenient Level 3 or 4 sea level anomaly (SLA) or sea surface height anomaly (SSHA) products (e.g., see Pujol et al., 2016, for examples of such products).

Thanks to new altimeter instruments and processing technology, the measured sea surface height (SSH) can retrieve smaller mesoscale features (e.g., Dufau et al., 2016) but it can only be exploited if the reference or MSS is as accurate as the SSH. Older MSS models were shown to be accurate enough to observe the larger mesoscale features (e.g., Dibarboire et al., 2011). But so far, the MSS errors have remained large in comparison with smaller mesoscale features (e.g., Dibarboire et al., 2012) and no error assessment has been performed specifically at the medium to small mesoscale.

In this context, the goal of this paper is twofold. First, it gives an overview of the new 2015 MSS model from the French Centre National d'Etudes Spatiales (CNES) and the company Collecte Localisation Satellites (CLS) that leverages more than 20 years of altimetry data, including 5 years of recent and precise geodetic data from Cryosat-2 and Jason-1 GM. This model was specifically developed to reduce the small-scale omission and commission errors observed in previous versions.

Second, this paper gives an overview of the breakdown of MSS errors for various scales, and specifically at the medium to small mesoscale. To gauge the improvement of the MSS model and its ability to observe small mesoscale features, we use recent and independent altimeter measurements. A new approach is also developed to quantify the MSS errors from medium wavelengths (less than 200 km) to small mesoscale wavelengths (less than 30–50 km).

The CNES_CLS15 MSS model is compared to its predecessor, the CNES_CLS11 model (Schaeffer et al., 2012), and to the latest model from the Danmarks Tekniske Universitet (DTU) detailed by Andersen

et al. (2015). For the sake of consistency, the three MSS models considered are referenced to the period 1993–2012.

The main differences between these models are the altimeter measurements used for their estimation. All the models were tested using measurements along historical repetitive tracks (Topex/Jason; Topex/Jason interleaved; ERS/ENVISAT; and GFO series). While only 1 year of geodetic measurement from ERS-1 was available for the CNES_CLS11 MSS estimation, the latest generation of models benefits from additional geodetic measurements: ENVISAT on its new orbit (DTU15 only), Cryosat-2 (the CNES model uses a basic Tracker mode processing over all regions where the delay-Doppler instrument mode is active), and the Jason-1 geodetic mission.

Another important difference concerns the MSS processing methodologies. The CNES_CLS and DTU also differ in the preprocessing of the altimeter measurements, in altimeter standards (e.g., retracker or geophysical corrections), as well as in the methodology used for intercalibration of the measurements from different altimeters and reduction of the ocean variability effect. These differences in the methodology, especially for small-scale signals, are discussed by Schaeffer et al. (2012) and Andersen et al. (2015).

The paper is organized as follows. An overview of the CNES_CLS15 model is given in section 2. The error assessment methodology is explained in section 3. The MSS models are analyzed and compared in section 4, and section 5 specifically considers an absolute error estimate with a focus on small mesoscale calculations.

2. Computation of the CNES_CLS15 MSS Model

2.1. Altimeter Data Processing

The CNES_CLS15 MSS computation is based on the 1 Hz SSH measured by different altimeters. The altimetric standards used in the reprocessed DUACS DT2014 products are used in this study. The details of the instrumental and geophysical corrections are described in Pujol et al. (2016).

As previously underlined by Schaeffer et al. (2012), the mitigation of the ocean dynamic variability is a key processing step. It makes it possible to retrieve the mean SSH component along the different tracks more accurately, but also to reference this mean SSH component to the same time period (also called the reference period), whatever the time period covered by the different altimeters. The methodology used to remove ocean variability from the altimeter measurement is the same as described by Schaeffer et al. (2012). It is essential along geodetic or long-repeat orbits whose time series are often limited to 1 or 2 years.

The delayed-time DUACS Level 4 gridded SLA DT2010 maps (Dibarbour et al., 2011) were used for this purpose. They were corrected to adjust the CNES_CLS15 MSS to the 20 year reference period, 1993–2012. Figure 1 illustrates the impact of this ocean variability correction. It shows the variance of the SLA signal along Cryosat-2 tracks, before and after removing the ocean variability. Before the application of this correction, the SLA variance characterizes the mesoscale variability, dominant in the western boundary currents and circumpolar current. In these areas, the SLA variance can reach more than 400 cm^2 . After the mitigation process, the bulk of the energy was removed, although a residual variability can still be observed (up to 80 cm^2 in high-energy areas). Indeed, the effective resolution of the DUACS gridded SLA maps is limited to wavelengths longer than about 200 km (Chelton et al., 2011) and this process does not accurately remove ocean variability at shorter wavelengths.

The different altimeter missions and periods used are summarized in Table 1. The corrected SSH measurements along geodetic tracks are used directly to estimate the MSS model. They include 4 years of Cryosat-2, 1 year of Jason-1 geodetic, and 1 year of ERS-1 data during its geodetic phase. The measurements along the repetitive tracks are used to estimate precise Mean Profiles (MPs), as described in Schaeffer et al. (2012). Computing the MPs enables us to reduce the signature of the small mesoscale signal not accurately removed previously, and the measurement noises, dominant at wavelengths shorter than nearly 65 km (Global mean estimation, Dufau et al., 2016). The CNES_CLS11 MSS is used to take into account the geoid cross-track gradients between the theoretical and observed measurement positions. They include slightly less than 21 cumulated years along the Topex-Poseidon/Jason-1/Jason-2 tracks, nearly 5 years along the Topex-Poseidon tandem/Jason_x02010;1 tandem tracks, nearly 15 years along the ERS-2/Envizat tracks, and nearly 7 years along Geosat Follow-On tracks.

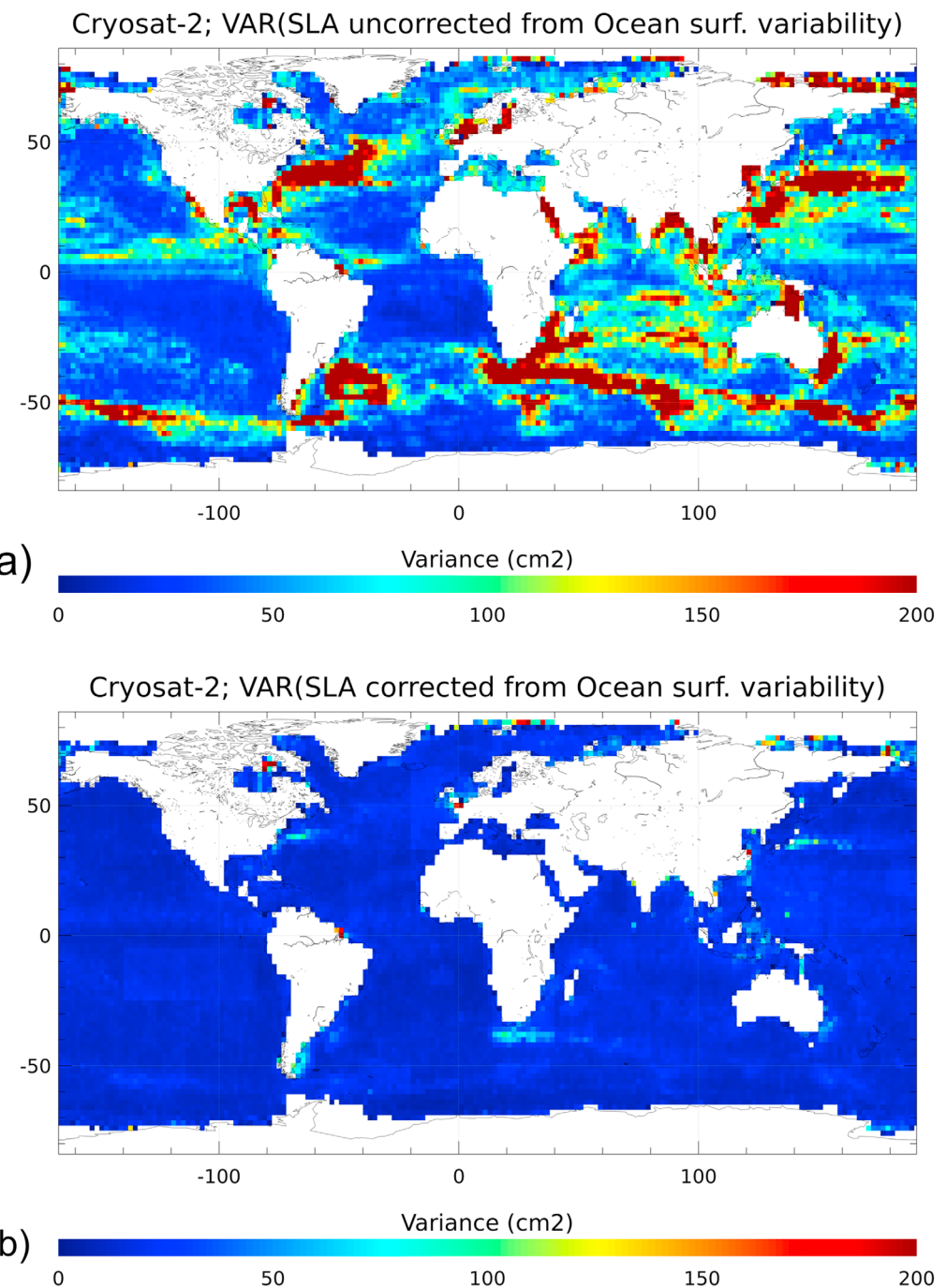


Figure 1. Variance of the SLA along Cryosat-2 tracks, (a) before and (b) after ocean variability mitigation. Statistics computed on $1^\circ \times 1^\circ$ boxes.

2.2. The CNES_CLS15 MSS—Collocation Methodology

The MSS models computed by CNES_CLS (1998, 2001, 2011, and 2015) are based on a suboptimal least squares collocation technique (e.g., Bretherton et al., 1976; Tarantola & Valette, 1982). Details of the method used to determine the CNES_CLS15 MSS model are described in Schaeffer et al. (2012) and further details are given in Hernandez and Schaeffer (2000, 2001).

Various important components have been improved over the 2011 model processing. In particular, the determination of the spatial correlation model, which still consists of two anisotropic components (North and East

Table 1
Altimeter Missions and Periods Used to Generate the MSS CNES_CLS15 Model

Satellite	Time period
T/P+Jason-1+Jason-2	1993–2012
TP Interleaved+Jason1 interleaved	Sep 2002 to Oct 2005 and Feb 2009 to Mar 2012
ERS-2+Envisat	May 1995 to Oct 2010
GFO	2001 to Aug 2008
ERS-1 geodetic	Apr 1994 to Mar 1995 (2 subcycles of 168 days)
Cryosat-2	2011 to May 2014
Jason-1 geodetic	May 2012 to Jun 2013

directions), is now based directly on SSH observations, especially to better take into account Cryosat-2 and Jason-1 geodetic data, which were not used for the CNES_CLS11 MSS calculation. It should be noted that more than 100 million data points have been integrated in this new CNES_CLS15 version: this is three times more than what was used for the 2011 version.

The new covariance model (adjusted anisotropic radii) was calculated on a 3 min resolution grid and is also defined for wavelengths between 5 and 150 km. In comparison, the model used for the former MSS was calculated on a 6 min grid and based on the contents of the CNES_CLS01 MSS, which used only the ERS-1 geodetic phase data for mapping the finest topographic structures.

The optimal interpolation methods used here are based on the remove/restore technique, with a correlation/covariance model tuned for wavelengths typically lower than 100 km. Previously, geoid models were used as reference field (e.g., first-guess). However, for greater consistency between the first-guess and the field to be determined, a filtered version of the CNES_CLS11 MSS for wavelengths greater than 100 km has been preferred.

As explained in Schaeffer et al. (2012), another major point of the preparation of MSS determination is the development and tuning of the noise budget associated with observations. The uncertainties budget used in the processing is described by three terms: an instrumental noise, a residual effect of the oceanic variability (in that case the goal is to take into account the residual variability presented in Figure 1), and an along-track bias.

From a statistical point of view, these three terms are complementary and correspond, respectively, to a white noise, a spatially correlated noise (at mesoscale wavelengths), and a long-wavelength error that is assumed to be constant along the tracks. Let us also remember that the quadratic sum of these three noises is adjusted to the standard deviation of the crossover differences, which enables us to obtain a calibrated formal error at the optimal interpolation output. Although the formal error is calibrated, it does not match the precision of the MSS but is nonetheless an excellent indicator of the consistency of the grid.

In practice, this formal error variance corresponds to a local minimum in the least squares sense; it depends on the spatial distribution and the density of the data used in the suboptimal estimation, but also on the noise budget. Overall, the map of this formal error gives us information about the homogeneity of the solution, and more locally the ratio between grid points is close to the relative accuracy.

If we consider the two maps shown in Figure 2, which highlight the formal errors of the CNES_CLS11 and the CNES_CLS15 MSS, respectively, we can observe that the new MSS is much more homogeneous and accurate than the former version. This is also confirmed by the world-wide statistics. The average of the formal error, which is 1.9 cm for the CNES_CLS11 version, decreases to 1.4 cm for the CNES_CLS15 MSS, and the standard deviation decreases even more strongly, from 2.1 cm to 1.3 cm.

3. Estimation of the MSS Error: Methodology and Data Used

In order to assess MSS errors at the large to medium mesoscale, a first analysis is made using 1 Hz measurements from different altimeters, as summarized in Table 2.

To quantify the relative error between two MSS models (see section 4), we use simple direct spectral estimates. Maps of the variance of the passband filtered SLA are also used to get a description of the geographical distribution of the error. In section 5, a more sophisticated strategy is used to derive the absolute error of each model. The extended methodology is detailed in Appendix A. Using the sum and difference of the SLAs from two cycles, we can infer the absolute MSS error if the cycles are selected to minimize the correlation between the dynamic fraction of the oceanic variability.

The following data sets are used throughout the paper:

1. One year from the Chinese/French HY-2A mission reprocessed by CNES (HPP products) (Jiang et al., 2012; Picot et al., 2013). This data is fully independent of all the MSS models considered: both the geographical location of the altimeter tracks and period are different from the MSS references.

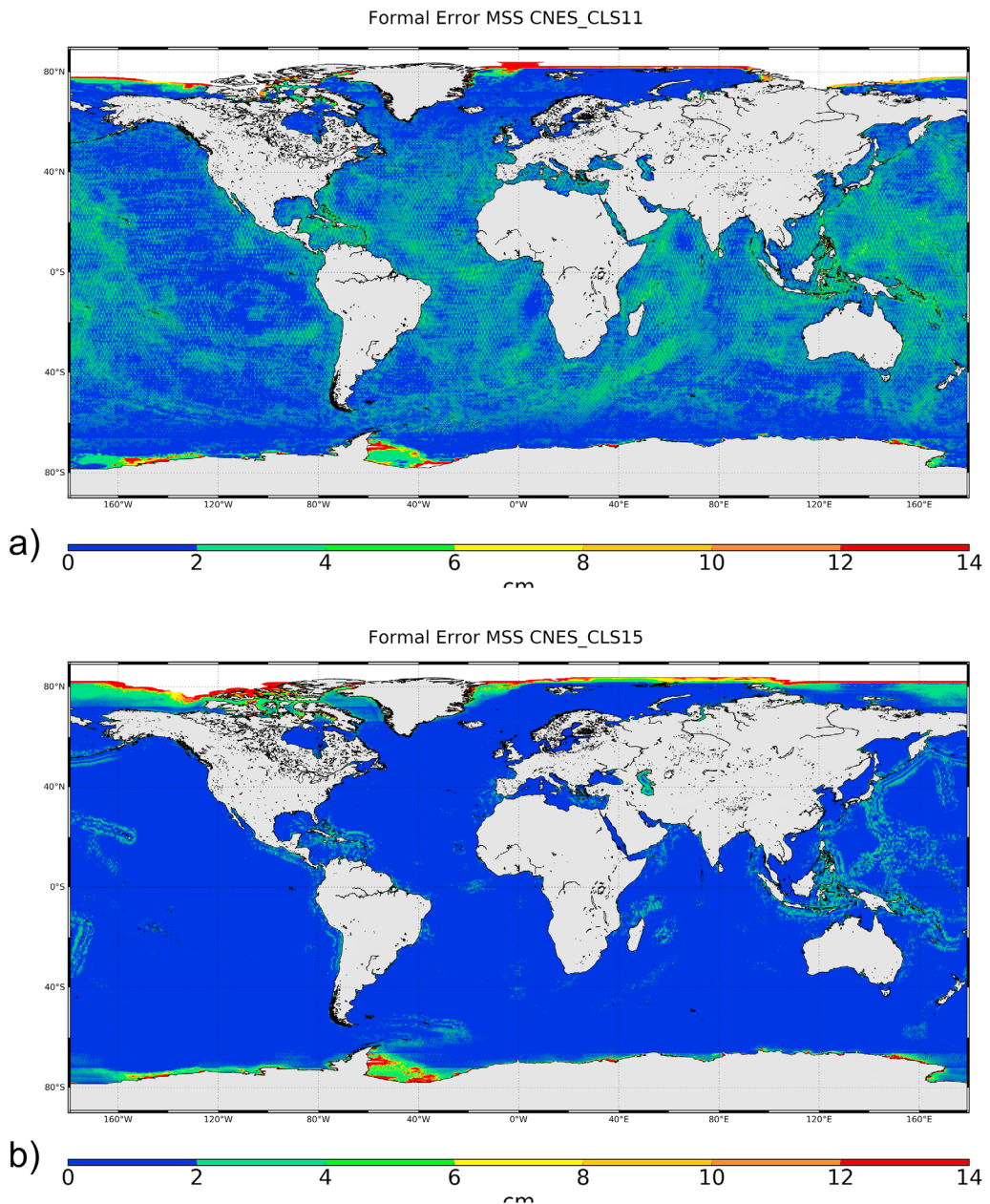


Figure 2. Formal error of the CNES_CLS11 (top) and CNES_CLS15 MSS models (cm).

Table 2
1 Hz and 20 Hz Altimeter Measurements Used for the MSS Errors Characterization

Satellite	Time period for 1 Hz measurement	Time period for 20/40 Hz measurement
Jason-1 interleaved	Apr 2011, May 2012	
Jason-1 geodetic	May 2012, Jun 2013	
Envisat geodetic	Nov 2010, Apr 2012	
SARAL/AltiKa (repetitive)	Jan 2015, Mar 2015	Cycles 10 and 15 (2014)
SARAL/AltiKa (drifting)	May 2015, Jul 2015	
HY-2A	Jan 2015, Dec 2015	
Sentinel-3A		Cycles 4 and 11 (2016)

2. One year of ENVISAT measurements during its geodetics phase. These measurements are not included in the CNES_CLS MSS computation but they are for the DTU15.
3. Three months of SARAL/AltiKa in 2015 when the satellite drifted away from the historical ERS/ENVISAT ground track. These measurements had not been used in any MSS model.
4. All Jason-1 geodetics (J1G) measurements. This data set is not independent of the MSS models, as it was used for both the 2015 models. Nevertheless, we use this knowledge to infer commission errors as detailed in Appendix B.

To focus on the smaller mesoscale, section 5 uses altimeter measurements from SARAL/AltiKa and Sentinel-3A. Both altimeters are very precise: the limited noise in the SSH makes it possible to assess dynamic signals at small scales (as opposed to a Jason-class altimeter where the altimeter noise floor would hide the values of interest), but that means using the full 20 Hz/40 Hz resolution.

Both Sentinel-3 and AltiKa are used over a period that was not included in the MSS model, but there is a major difference between the two data sets. AltiKa is operated exclusively along an historical repetitive track (or charted track) where more than 20 years of altimeter measurements (ERS/ENVISAT series) provide a very precise description of the local one-dimensional MSS. In contrast, Sentinel-3 is operated on a new orbit, i.e., on a ground track where the MSS model is constructed without this very precise time series (uncharted ground track).

The AltiKa data set is derived from the Prototype for Expertise on AltiKa for Coastal, Hydrology and Ice (PEACHI) project from CNES (Valladeau et al., 2015). We specifically use Cycles #10 (February 2014) and #15 (August 2014) to benefit from the decorrelation described in Appendix A. The Sentinel-3 data were derived from the CNES S3 processing prototype (S3PP v1.2; Boy et al., 2017.) used to support the commissioning phase of the mission. Cycles #4 (May 2016) and #11 (Nov 2016) were selected to benefit from the decorrelation described in Appendix A.

4. Comparing the Errors of Recent MSS Models

4.1. Improvements Observed With the 2015 Models

Figure 3a shows the mean global SLA power spectral density (PSD) along HY-2A tracks when different MSS models are used. All PSDs are superimposed for wavelengths longer than 150 km but differences become visible at shorter wavelengths: there is less energy in the SLA based on the 2015 MSS models.

Because the SSH and MSS are based on independent data and periods, one can assume that the energy difference originates in errors from the 2011 MSS models that have been removed in newer models (see Appendix B). This improvement is significant from ~25 to 170 km. For smaller wavelengths, the altimeter noise floor dominates, and for longer wavelengths, the difference between MSS models is marginal with respect to the variance of the SLA signal itself.

To better quantify the differences between the MSS models, Figure 3b shows the ratio between the PSD curves of Figure 3a. Compared to the CNES_CLS11 MSS, the CNES_CLS15 MSS improves the SLA signal mainly at wavelengths ranging from 20 to 200 km with a maximal impact around 60 km, while the 2015 model reduces SLA variance by approximately 15%.

Table 3 also gives the SLA variance in cm^2 for wavelengths ranging from 20 to 200 km along different altimeter tracks and for the three MSS models. Along HY-2A tracks, the mean global SLA variance reduction is 0.81 cm^2 when using CNES_CLS15 instead of the 2011 version, i.e., nearly 8% of the SLA variance (using CNES_CLS15 MSS).

Almost the same spectral signature (not shown) and same mean variance reduction are observed along other independent tracks such as Envisat on its End-of-Life orbit and SARAL/AltiKa during its 3 month drift in 2015 (maximal drift reaching slightly more than 10 km from its nominal ground track position at the equator). For these two ground track positions, the mean variance reduction at 20–200 km wavelengths is, respectively, 0.63 cm^2 (7.2%) and 0.61 cm^2 (6.5%) (Table 3).

The improvement of these values world-wide should be compared to the level of white noise in the altimeter data. The noise floor of a Jason-class altimeter is of the order of 2.7 cm (Zanife et al., 2003) whereas a Sentinel-3 or AltiKa-class altimeter has a noise floor that ranges between 1.5 and 2 cm .

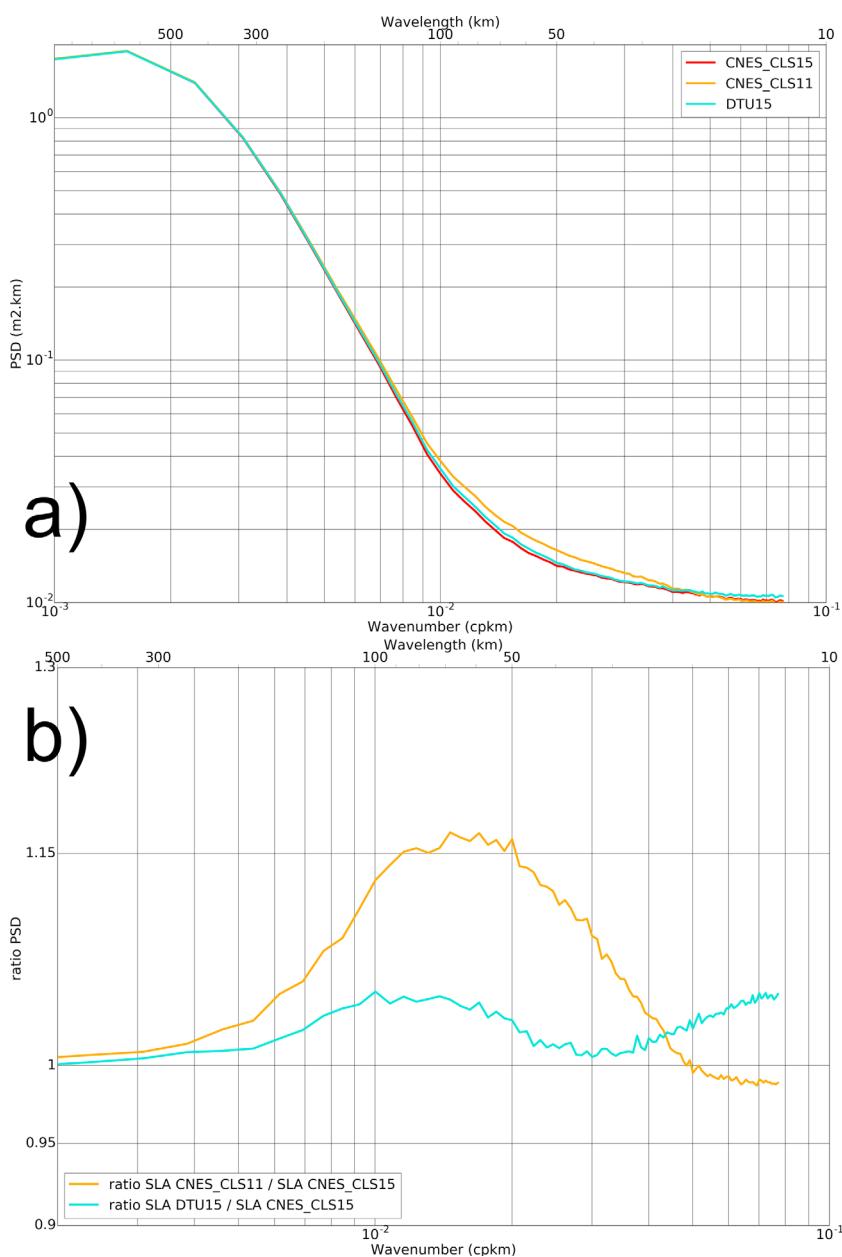


Figure 3. (a) The SLA PSD along H2 tracks using several MSS models: CNES_CLS15 (red), CNES_CLS11 (yellow), DTU15 (cyan). (b) The ratio of SLA spectra from panel (a): PSD(SLA with CNES_CLS11)/PSD(SLA with CNES_CLS15) (yellow) and PSD(SLA with DTU15)/PSD(SLA with CNES_CLS15) (cyan).

Table 3

Variance of the Short Wavelengths 1 Hz SLA Along the Track of Different Altimeters, and Using Different MSS Solutions (Passband Filtered From 20 to 200 km)

	Jason-1 interleaved	Jason-1 geodetic	Envisat geodetic	SARAL/AltiKa (repetitive)	SARAL /AltiKa (drifting)	HY-2A
CNES_CLS11	10.42	11.26	9.36	8.69	9.94	10.93
CNES_CLS15	10.12	9.33	8.73	8.71	9.33	10.12
DTU15	10.67	9.47	8.34	9.01	9.05	10.36

Note. The figures for independent data sets (not used in the MSS models) are highlighted in bold. (Units: cm^2).

Moreover, these world-wide values hide a considerable geographical variability. Figure 4 shows a map of the SLA variance reduction for wavelengths shorter than 250 km and along HY-2A tracks. Because the SSH from HY-2A is independent of the data used in the MSS, any variance removed (positive values) can be related to an improvement of the 2015 MSS model with respect to the 2011 version (Appendix B). Conversely, a negative value means that the variance increased with the 2015 model, i.e., that the MSS error is locally higher.

Figure 4a shows that error reduction occurs mainly along geodetic structures, where it reaches more than 2 cm². This is an omission error of the 2011 model that is now resolved with the 2015 model because it leverages 5 years of dense geodetic data. To put these figures into perspective, along these geodetic features, the improvement from the 2011 to the 2015 model can locally contain more energy than the Sentinel-3 noise floor. These figures underline how valuable the improvement of new MSS models is, and especially for new altimeter technology operated on uncharted ground tracks such as Sentinel-3 (or SWOT).

Furthermore, an important result visible in Figure 4a is that the map is almost entirely positive: even the western boundary currents and circumpolar regions show no negative values. Using geodetic data sets to build an MSS model is generally trickier than using mean profiles along a repetitive track. The former contain far more oceanic variability than the latter: a simple 20 year average along the TOPEX/Jason track averages out natural variability and is equal to the local MSS model. The 2015 model uses 4 years of Cryosat-2 and 1 year of Jason-1-GM data, i.e., much more geodetic data than the 2011 model. If the ocean variability was not properly mitigated, it would introduce commission errors in the 2015 MSS models, i.e., a degradation with respect to the 2011 model (negative values in Figure 4a). To that extent, the positive values of Figure 4a show that the leakage of residual ocean variability in the CNES_CLS15 model is smaller than the omission error of the 2011 model. However, section 4.4 will show that this leakage is still present in all MSS models.

4.2. Comparison Between the CNES_CLS and DTU Models

Figure 4b shows a similar comparison between the DTU15 model and the CNES_CLS15 model. Again, because HY-2A is an independent data set, a variance reduction (or positive value in Figure 4) means that the CNES_CLS15 model locally has a smaller error than the DTU15 one. Conversely, negative values mean the DTU15 mode is locally better.

Figure 4b shows that the CNES_CLS15 model has smaller errors over mesoscale-active regions (e.g., Western boundary currents). This might be explained by differences in the processing of the ocean variability (discussed in sections 2.1 and 4.4, as well as in Schaeffer et al., 2012). Conversely the DTU15 model is more accurate in the Indonesian region and in a small set of specific pixels located on intense gravimetric structures. One can speculate that the difference originates in actual valid altimeter measurements that had been rejected from the CNES_CLS MSS mapping process because they were incorrectly flagged as outliers.

In addition to the differences observed at short wavelengths, the CNES_CLS15 and DTU15 models also exhibit differences at wavelengths longer than 200 km (Figure 5): between 60°N and 60°S, there are significant differences in the main ocean circulation patterns and mesoscale-active regions (e.g., Gulf Stream, Kuroshio, Agulhas Currents). For wavelengths longer than 1,000–5,000 km, geographically coherent differences of the order of 1–2 cm can also be observed in most regions. There is also a bias of 5 cm or more at latitudes higher than 60–70°: this bias is specifically discussed in section 4.6.

Dibarboire et al. (2012) have shown that the different methodologies used for the ocean variability correction used by DTU and CNES/CLS can explain most of the differences observed in Figure 5. As explained in section 2, the ocean variability correction is an important preprocessing step used before the merging of all the altimeter measurements from different periods (e.g., TOPEX/Jason series available from 1993 to 2014, as opposed to Cryosat-2 available only from 2011 to 2014). This process ensures that the MSS model is representative of the chosen period (e.g., from 1993 to 2012 for the CNES15 model) and that the influence of high-frequency, seasonal and interannual variability is mitigated.

Table 4 gives the standard deviation of Sentinel-3A sea level anomalies (independent altimeter and period): one can observe a variance reduction of approximately 2.4 cm RMS when the CNES_CLS15 model is used in global ocean, whereas the variance reduction is only 0.6 cm for latitudes higher than 66°N. In other words, for wavelengths longer than 100–200 km, the preprocessing used for the CNES_CLS model is more efficient than for the DTU model, but it becomes less effective at higher latitudes where both models likely have a similar large scale accuracy. One could argue that the selection criteria applied, which implies the use of a MSS for

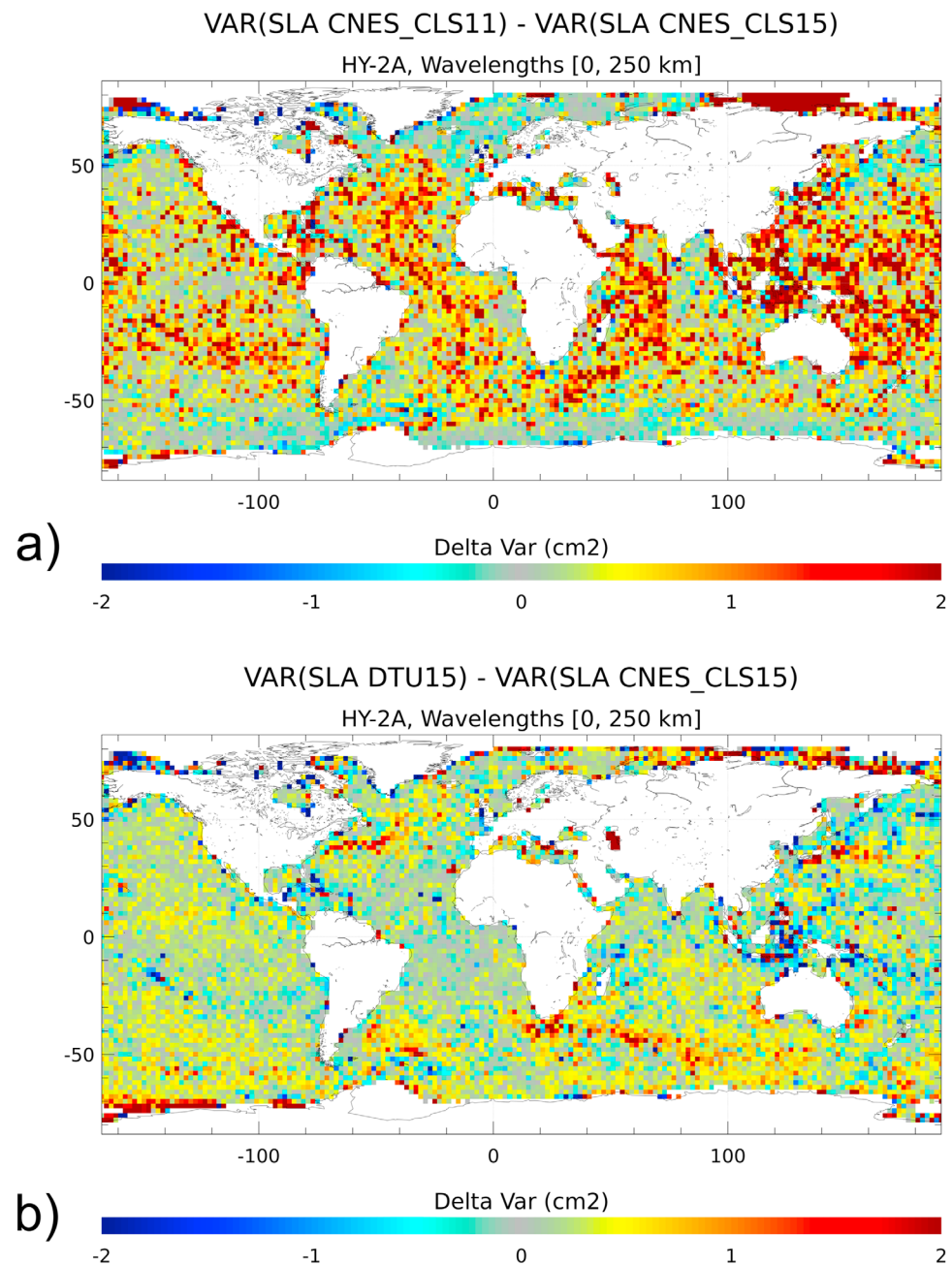


Figure 4. Difference of the SLA signal variance (a) from CNES_CLS11 to CNES_CLS15 or (b) from DTU15 to CNES_CLS15 along HY-2A tracks. The SLA was high-pass filtered to keep only wavelength shorter than 250 km.

the SLA criteria, could give advantage to this particular MSS (here MSS CNES_CLS15 used in selection criteria). Additional sensitivity tests, applying selection criteria that use both the MSSs, underlined that even if the level of SLA variance depends on the editing strategy, the conclusions remain unchanged.

4.3. Variability Around a Charted Track

Due to platform anomalies onboard SARAL/AltiKa, the altimeter left its nominal 1 km ground track for approximately 3 months. This event yielded a unique data set with respect to the analysis of the MSS error: in this section, we use this independent AltiKa data set to quantify the MSS model error as a function of the cross-track distance to the historical charted ground track.

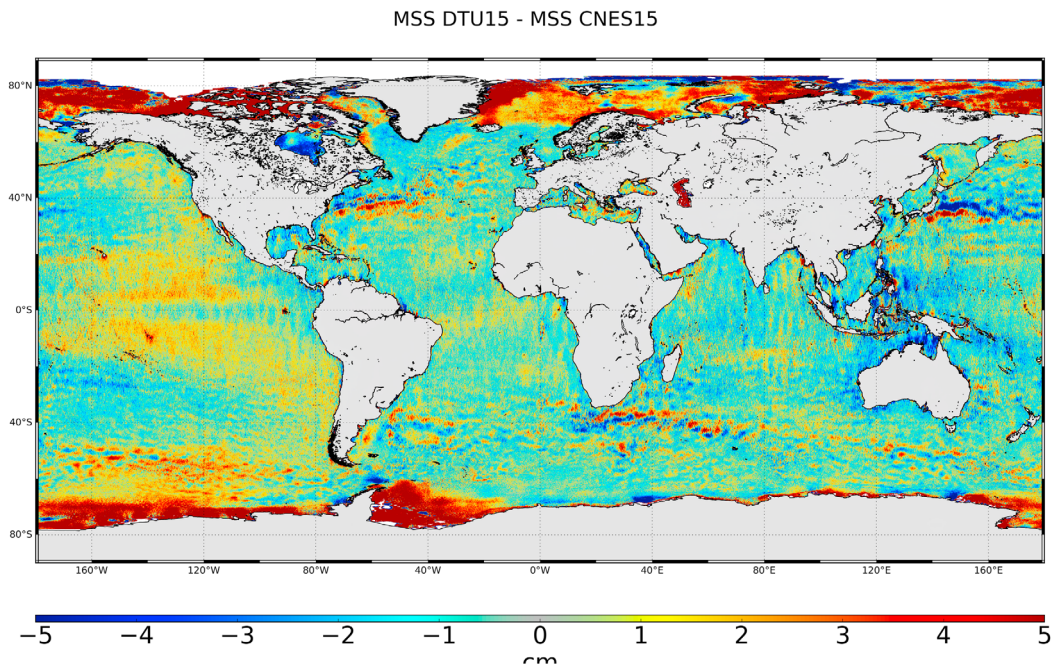


Figure 5. Difference between the MSS DTU15 and CNES15 models (units in cm).

The dark blue curve of Figure 6b shows the temporal evolution of the AltiKa cross-track distance between the observed position and its repetitive theoretical track position. The nominal value ranges from -1 to $+1$ km, except in May to August 2015, when the satellite went as far as 10 km off-track.

The black curve of Figure 6a shows the Jason-2 SLA standard deviation for wavelengths shorter than 200 km. The region used is in the Tropical Atlantic Ocean for two reasons: the geoid and MSS features are relatively complex (the omission error is not zero) and mesoscale variability is weak enough for us to clearly quantify MSS model errors in SLA variance differences. In this region, the Jason-2 SLA has a standard deviation ranging from 2.1 to 2.7 cm. Because Jason-2 is very stable on its reference track, we can use this curve as a reference to gauge actual variations in the natural oceanic variability of this region and period.

The red, cyan, and orange curves of Figure 6a show the AltiKa SLA standard deviation using various MSS models. All these curves are approximately 0.5 cm below the Jason-2 black curve. This is expected and related to the lower noise floor of AltiKa (e.g., Dufau et al., 2016).

As for Jason-2, the AltiKa curves show a substantial amount of natural variability. When AltiKa is along its nominal ground track, the Jason-2 and AltiKa curves are very similar (not perfectly identical, as the satellite tracks are different). During this period, the DTU15 MSS exhibits slightly more error than the CNES_CLS models (the cyan curve is significantly above the red and orange curves). In other words, the DTU15 model is slightly less precise than CNES_CLS models along the charted tracks of historical orbits with a difference in the region of 0.1 cm RMS (wavelengths shorter than ~ 200 km).

In contrast, when AltiKa departs from its nominal ground track (May–August), the standard deviation of the AltiKa SLA increases, whereas it is very stable for Jason-2. This difference is due to a higher MSS error in all models when AltiKa departs from the charted ground track. The increase is very clear for the CNES_CLS11 model in orange, and smaller for the 2015 models.

Natural oceanic variability makes the MSS error relatively hard to quantify on each curve of Figure 6a. Therefore, Figure 7a shows the difference of SLA variance between Jason-2 and AltiKa as a function of the ground track position. The marker colors are the date of each point. During most of the 2015 period, AltiKa stays within 1 km of its

Table 4

Sea Level Anomaly (SLA) Mean and Standard Deviation (STD) Along Sentinel-3A Tracks for Different Latitude Bands

SLA Mean/STD	DTU15	CNES-CLS15
Global Ocean	$-2.31/10.17$	$-2.30/9.88$
66°S – 66°N	$-2.18/10.15$	$-2.31/9.90$
Above 66°N	$-4.45/8.98$	$-2.05/8.96$

Note. The SLA is referenced to the CNES15 (left column) or DTU15 (right column) MSS model. (Units in cm). Computed on a common measurement coverage (only on pixels defined in both MSS models and using measurement selection criteria defined in Eumetsat products).

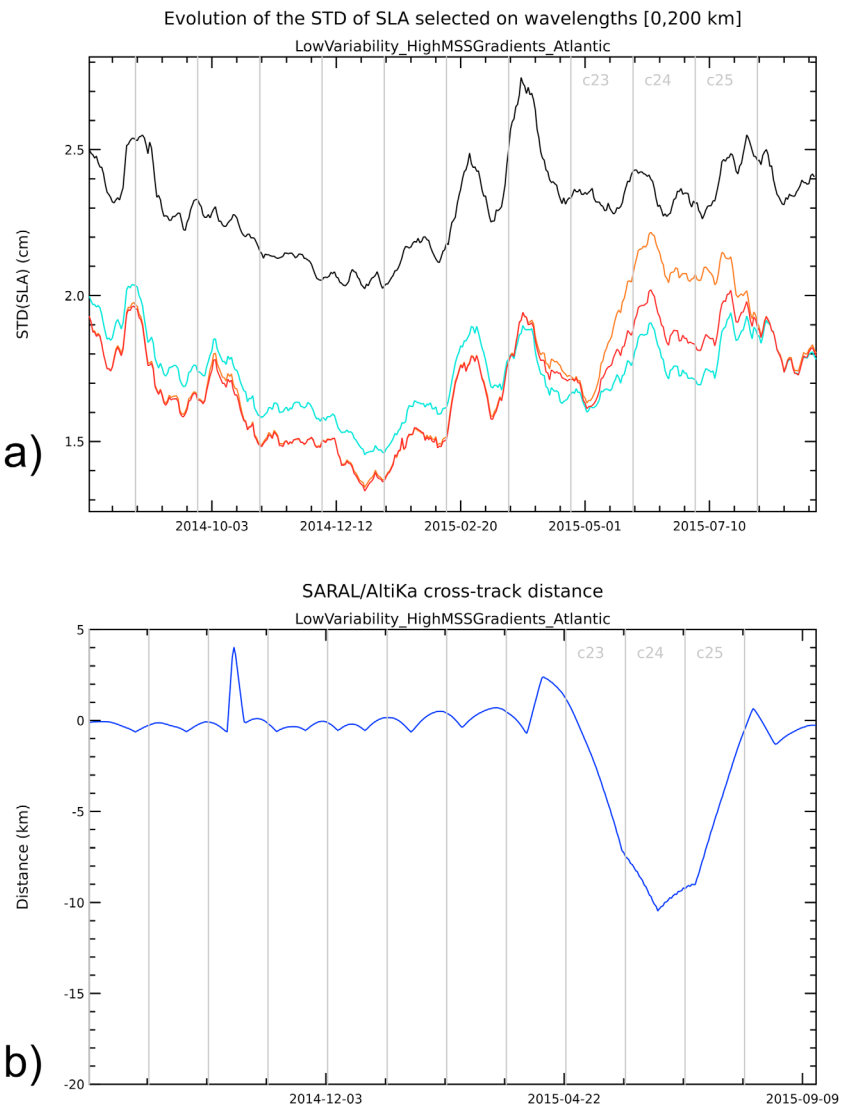


Figure 6. (a) Temporal evolution of the standard deviation of the SLA, along Jason-2 track (black) and SARAL/AltiKa tracks when MSS CNES_CLS15 (red), CNES_CLS11 (orange), and DTU15 (cyan) is used. The SLA was high-pass filtered to keep only wavelengths shorter than 200 km. Statistics computed over a low variability and intense bathymetric gradients areas [$-20, 0^{\circ}\text{N}$; $-30, 0^{\circ}\text{E}$]. (b) Cross-track distance at the equator between the SARAL/AltiKa observed position relative to its theoretical track (right axis). The gray vertical lines delimit the period for the different AltiKa cycles. The drift of the AltiKa ground track position occurred between cycles 23 and 25.

nominal track (cluster of points with an abscissa close to zero). This period gives an idea of the natural variability seen in the Jason/AltiKa differences (gray box) of the order of $\pm 0.7 \text{ cm}^2$.

However, from May to August (orange to light red symbols), the ground track departs from its nominal value. In both cases the SLA variance difference between AltiKa and Jason-2 increases linearly with the cross-track distance. This is a direct measurement of the CNES_CLS_11 MSS error away from charted tracks. The regression coefficient is $1.8 \text{ mm}^2/\text{km}$ (or $0.42 \text{ cm RMS per km}$). While this coefficient might seem small, the 10 km departure of SARAL during this period results in a 1.7 cm^2 variance increase in AltiKa SLA products. Note that this order of magnitude is consistent with the observations and predictions of Dibarbour et al. (2012).

The same analysis with the CNES_CLS15 MSS is shown in Figure 7b. The SLA variance increase is smaller but still visible (of the order of 0.3 cm RMS/km). Thanks to the addition of smaller scales from the geodetic data

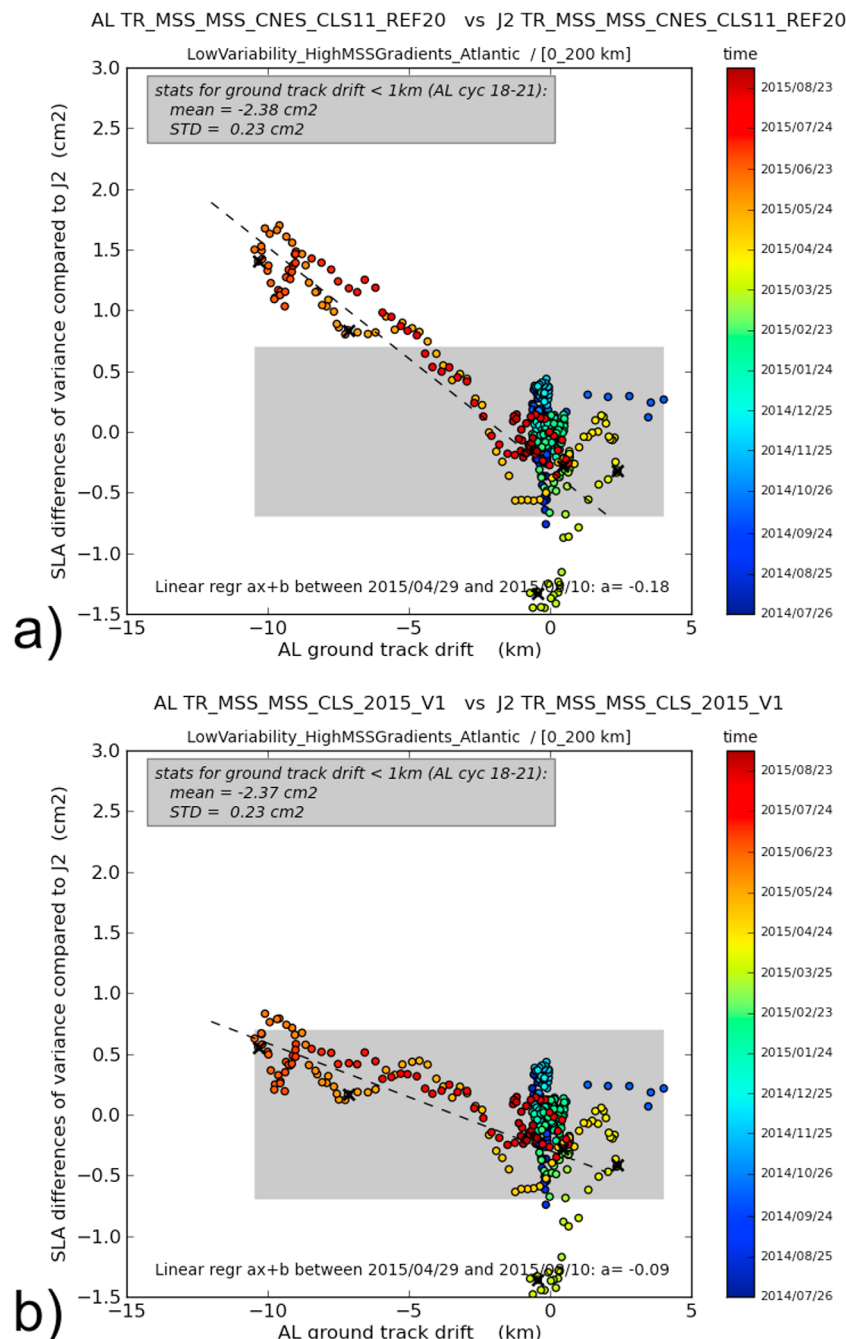


Figure 7. Difference of the variance of the SLA signal observed along Jason-2 track or SARAL/AltiKa tracks as a function of the cross-track drift with respect to its theoretical position. The SLA is high-pass filtered (200km) and computed using the (a) MSS CNES_CLS11 and (b) CNES_CLS15, over a low variability and intense bathymetric gradients areas [-20, 0°N][-30, 0°E]. Gray box corresponds to the variance differences observed that can be statistically explained by the ocean variability.

set, the new generation of MSS models is much more homogeneous when a satellite departs from its nominal 1 km band, whereas older MSS models exhibited a substantial error increase away from charted tracks.

The region analyzed features a rather rugged bathymetry and very little mesoscale variability, so one can speculate that in the global ocean, a deviation of 1–5 km would be barely detectable with a Jason-class altimeter. This is very desirable from an operational point of view: if another satellite were to drift away

from its nominal track as AltiKa did in 2015 due to an onboard constraint, the impact would be marginal for operational oceanography (e.g., Le Traon et al., 2014).

4.4. Commission Error From Ocean Variability

As discussed in section 2, the correction of the dynamic ocean variability has a significant impact on the accuracy of the MSS estimated. When nonpermanent dynamic eddy structures are not completely removed in the processing, they can be misinterpreted as a permanent MSS feature. In addition to the true mean SSH, the MSS model may absorb a small fraction α of the SLA of this event.

$$\text{MSS}_{\text{model}} = \text{MSS}_{\text{true}} + \alpha \cdot \text{SLA}_{[t_0, t_0']}$$

As detailed in Appendix B, this leakage of ocean dynamics into the MSS model results in two types of errors:

1. When the period is the same as the event, any SLA computed with the MSS model corrupted with ocean variability leakage will lose a fraction of its variance because the reference contains a fraction of the dynamic signal that should be in the SLA instead of the MSS. This can be the case for Cryosat-2 or Jason-1 GM:

$$\text{SSH}_{[t_0, t_0']} - \text{MSS}_{\text{model}} = (1 - \alpha) \text{SLA}_{[t_0, t_0']}$$

2. When the period considered is different, the MSS error artificially creates additional variance in the SLA computed with this model (e.g., Sentinel-3 or HY-2A). This is because the SLA leakage into the MSS model is different from the SLA for this time period:

$$\text{SSH}_{[t_1, t_1']} - \text{MSS}_{\text{model}} = \text{SLA}_{[t_1, t_1']} + \alpha \cdot \text{SLA}_{[t_0, t_0']}$$

The difference between these two effects is very important because we can use it to determine whether the MSS error observed originates in omission errors or commission errors from ocean variability. To do this, we can use the orbit change between Jason-1 interleaved (historical track charted with TOPEX) and Jason-1 GM (geodetic uncharted track). Indeed, the Jason-1 GM data were used in the 2015 model, so we can infer whether its SLA variance increases (omission error of the MSS) or decreases (commission error, ocean variability from geodetic data has leaked into the MSS model).

Figure 8 shows the evolution of the high-pass filtered SLA variance along Jason-1 and Jason-2 tracks using MSS calculated by CNES_CLS15 and DTU15. The first part of the period considered here corresponds to the interleaved phase of Jason-1. During this period, we can observe good consistency between the SLA variance defined along Jason-2 and Jason-1 interleaved tracks.

Note that, as for AltiKa in Figure 6, the gray and cyan curves (SLA with DTU15) are slightly but clearly above the black and red ones: along charted historical tracks of TOPEX/Jason, the DTU15 model is less accurate than the CNES_CLS models based on mean profiles. The additional error is of the order of 0.1 cm RMS (consistent with the observations from AltiKa).

The second period of Figure 8 corresponds to the geodetic phase of Jason-1 (Jason-1 GM). In this case, we observe a clear decrease of the variance of the SLA along Jason-1 GM tracks while the variance along Jason-2 tracks remains quite stable. The variance is lost for both MSS models, but the variance loss is clearly more pronounced in the cyan curve of the DTU model.

With the CNES_CLS15 MSS, the SLA variance loss (leakage of oceanic variability into the MSS) is 1 cm², i.e., 9.3% of the variance observed along Jason-2 tracks. For the DTU15 model, the variance loss is almost twice as high, at 1.9 cm² (17%).

4.5. Coastal Regions

The MSS errors were assessed in the coastal areas using independent HY-2A 1 Hz measurements (Table 2). Figure 9 shows the global standard deviation of the SLA (all wavelengths included) as a function of the

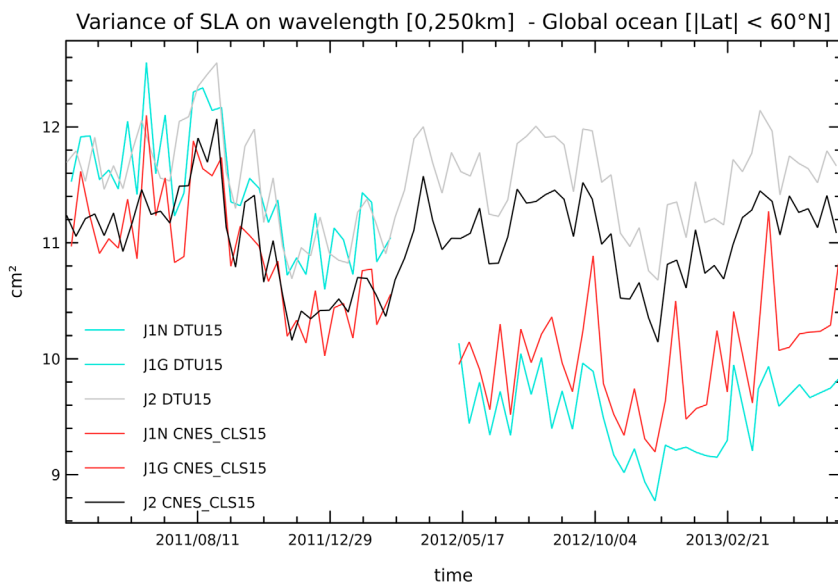


Figure 8. Temporal evolution of the SLA variance along the tracks of Jason-2 (J2) and Jason-1 interleaved (J1N) and geodetic (J1G) phases. The SLA was high-pass filtered (250 km) and estimated using MSS CNES_CLS15 (black and red lines) and DTU15 (gray and cyan lines).

distance to the coast for different MSS models. For all MSS models, we can see an increase in the SLA variance in coastal regions (30 km or less from the coastline). This extra variance may have three origins:

1. True coastal features (e.g., currents and eddies).
2. Errors in the SSH measurements (altimeter range, wet troposphere radiometer correction, other geophysical corrections such as tidal models).
3. Errors in the MSS models.

As in Figure 6, the different behavior observed for the three MSS models using common HY-2A data makes it possible to quantify the error difference between two models (but not the absolute error, as it is not possible to disentangle the three terms above).

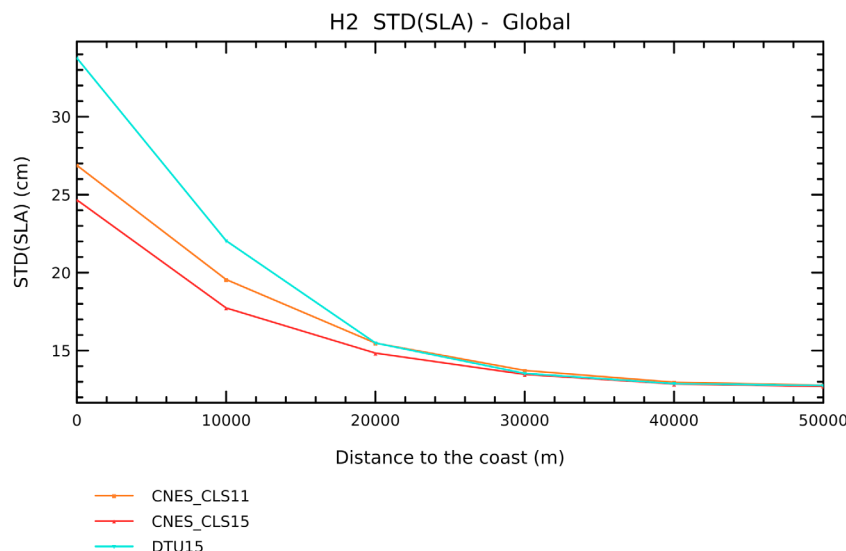


Figure 9. Variance of the SLA signal along HY-2A tracks as a function of the distance to the coast. SLA is computed using MSS CMES_CLS11 (orange), CNES_CLS15 (red), and DTU15 (cyan).

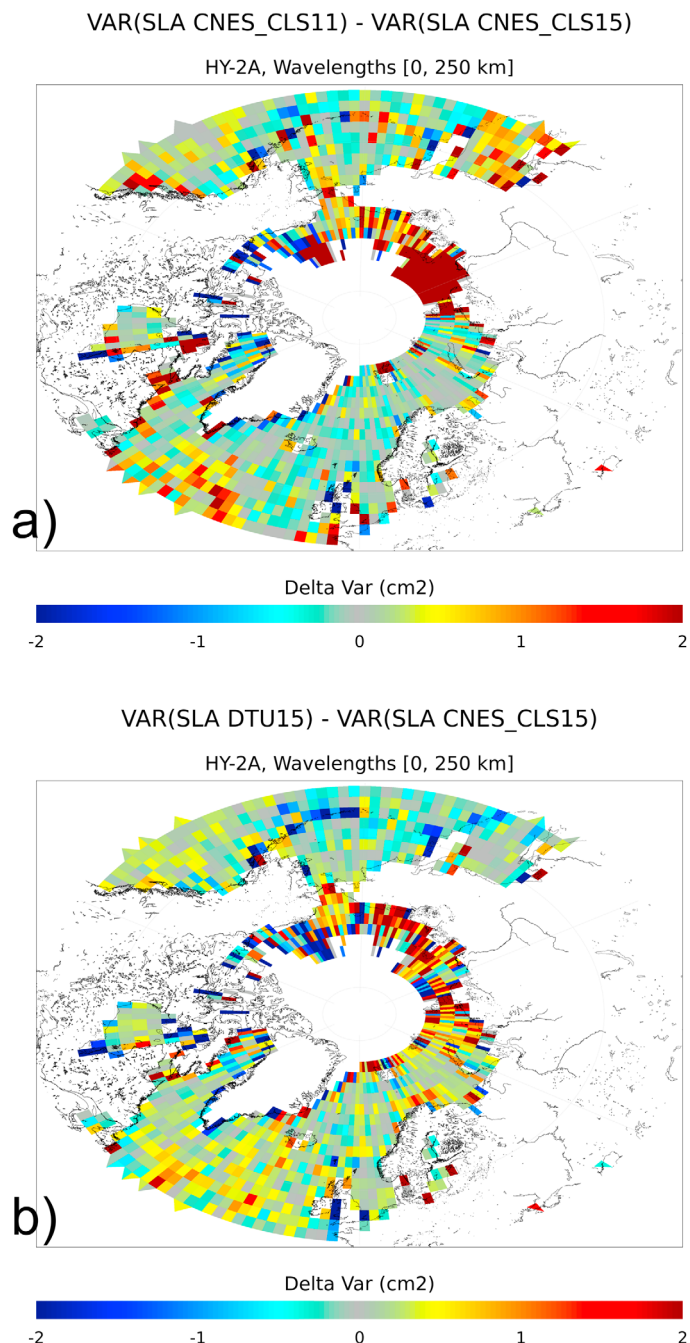


Figure 10. Same as Figure 4 with zoom on the Arctic Region.

Figure 9 shows that the coastal variance increase is smaller with the CNES_CLS15 MSS, illustrating the globally improved accuracy of this MSS in coastal regions. At 10 km from the coast, the mean SLA variance observed with the CNES_CLS15 MSS is close to 314 cm^2 . It is more than 68 cm^2 lower than the variance observed with the CNES_CLS11 MSS, which accounts for about 20% of the variance observed with the CNES_CLS15. Compared to the DTU15, the CNES_CLS15 model contributes to reducing the SLA variance by more than 171 cm^2 (10 km from the coast), i.e., nearly 55% of the variance observed with the DTU15 MSS.

4.6. Arctic Region

Figure 10 shows the difference of the short wavelength (<250 km) SLA variance over the Arctic region, when computed with the CNES_CLS15 and CNES_CLS11 MSS or the DTU15 MSS along HY-2A tracks during the year 2015. The comparison between the CNES_CLS15 and CNES_CLS11 (Figure 10a) highlights an overall reduction of the SLA variance with the new MSS (positive values on the figure), especially intense in the Siberian Sea where the CNES_CLS11 MSS was mainly based on the geoid information. The variance reduction reaches more than 2 cm^2 for wavelengths shorter than 250 km. It can reach more than 20 cm^2 over the whole wavelength spectrum (not shown).

No specific processing was implemented for the CNES_CLS15 MSS estimation in the high latitude areas. Nevertheless, compared to the previous version (CNES_CLS11), the CNES_CLS15 MSS model benefits from more and better altimeter measurements in these regions, where they significantly contribute to improving the MSS accuracy.

The comparison between CNES_CLS15 and DTU15 (Figure 10b) shows that locally the DTU15 strongly contributes to reducing SLA variance (negative values on the figure). This is especially the case in the northern Canadian and Beaufort Seas or along the Greenland coasts. Nevertheless, elsewhere we can observe the positive impact of the CNES_CLS15 MSS (positive values on the figure), with a reduction of the variance of SLA in the Siberian Sea.

When looking at longer wavelengths, the differences between the CNES_CLS15 and DTU15 models can be very large in the Arctic region (Figures 5 and 11a).

First, the coverage between the two MSS models is different. The CNES_CLS15 models are based on altimeter measurements from the open ocean. As a consequence, it is not defined in all regions where measurements are not available (e.g., permanently covered by ice during the period ranging from 1993 to 2014) and/or rejected on selection criteria (e.g., over sea ice areas). The boundaries of the CNES_CLS15 coverage are highlighted with a red line in Figure 11a. In contrast, the DTU15 model is defined up to 90°N .

Second, an offset between both models can be observed in the MSS differences near 66°N in the Atlantic Ocean (Figure 5). It is perfectly East/West oriented and located at the limit of the Topex/Poseidon orbit coverage. As no known physical signal presents the same characteristics, this gradient can be defined as unrealistic and probably induced by a weakness of the missions intercalibration processing. This meridional gradient originates in one of the MSS models or in both of them. In order to quantify the amplitude of the offset in each model, we computed the mean of Sentinel-3A SLA separating latitudes lower and higher than 66°N . The results are given in Table 4: the mean is approximately -2 cm for both models below 66°N and -2 cm

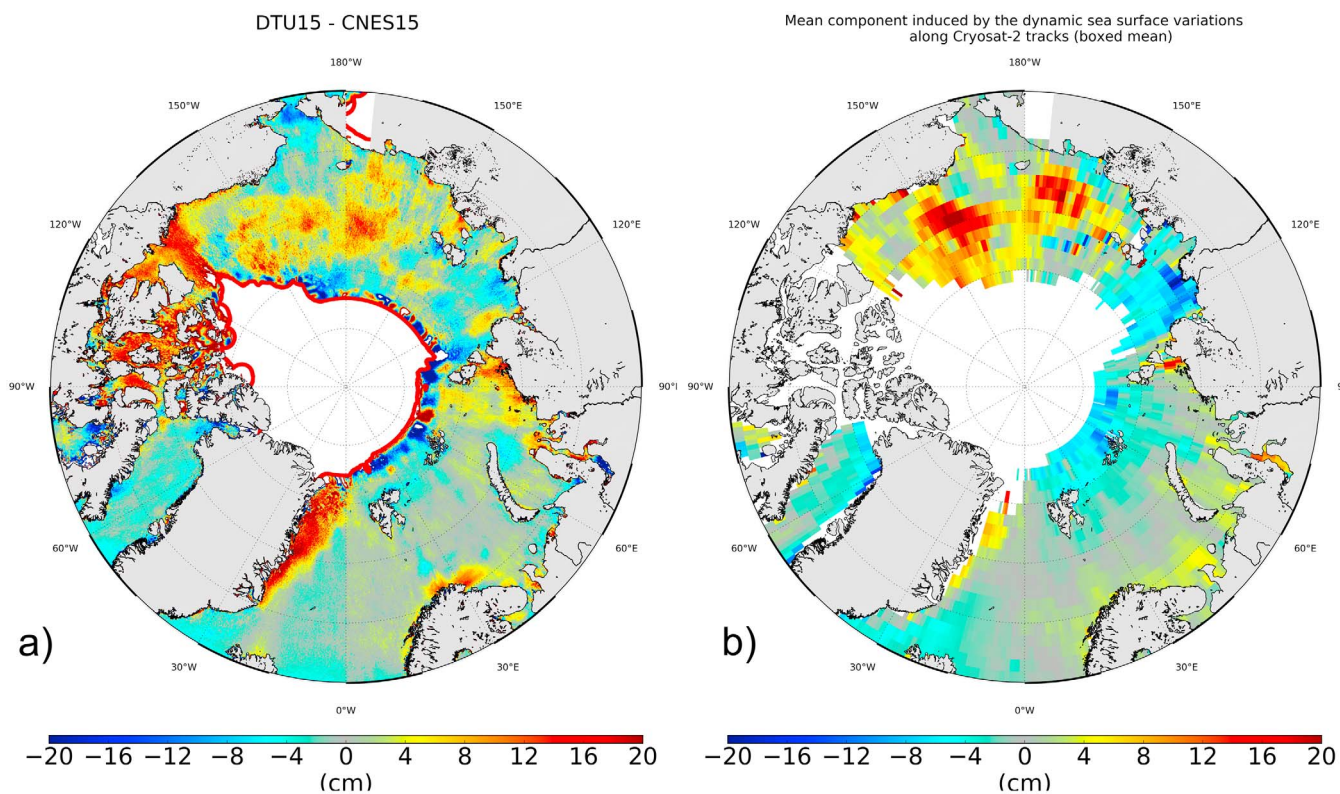


Figure 11. (a) Difference between the MSS DTU15 and MSS CNES15 in the Arctic Region. The limits of the MSS CNES15 is shown with the red line. (b) Mean component induced by the ocean variability estimated along Cryosat-2 tracks (boxed mean).

above 66° for the CNES_CLS15 model. At low latitudes, both models are consistent, and the cross-calibration preprocessing used for the CNES_CLS15 model (see section 2, Le Traon & Ogor, 1998; Pujol et al., 2016) is creating a seamless transition between the TOPEX/Jason data coverage and the other altimeters. In contrast, the mean SLA is -4.5 cm for the DTU model above 66° N. In other words, the offset visible in Figure 5 is primarily due to DTU15. Furthermore, the standard deviation of the Sentinel-3A sea level anomaly (Table 4) is significantly lower for the CNES_CLS15 model below 66°, and it is approximately the same for both models above 66°. In other words, the seamless transition near 66° in CNES_CLS15 is good because it avoids a likely unrealistic MSS gradient, but it may not significantly improve the model accuracy in the Arctic Ocean.

Lastly, geographically coherent patterns are visible in regions seasonally covered by sea ice (Figure 11a). They can be as high as 15 cm or more. Estimating the MSS in these areas is quite difficult due to the sparsity, seasonality, and lower quality of altimeter measurements. In these regions, it is also more challenging to mitigate the influence of the ocean variability, and to account for seasonal signals (altimeter coverage is denser in summer, i.e., potentially skewing the MSS model if the effect is not accounted for).

Figure 11b illustrates this effect. It shows the mean ocean variability estimated along CryoSat-2 tracks (estimated from DUACS DT-2014 gridded products, as per section 2). This map exhibits geographically correlated patterns with an amplitude as high as 15 cm or more. These regional biases created by the oceanic variability are similar to various patterns in Figure 11a: in the Occidental Siberian Sea and Laptev Sea, a significant fraction of the MSS model mismatch originates in different methodologies to mitigate the oceanic variability.

Nevertheless, oceanic variability does not explain all the differences observed between the two MSS models. Other differences could be explained by the use of different altimeter data sets: different retrackers, data selection in sea ice covered regions, exact periods used, corrections (e.g., sea state bias).

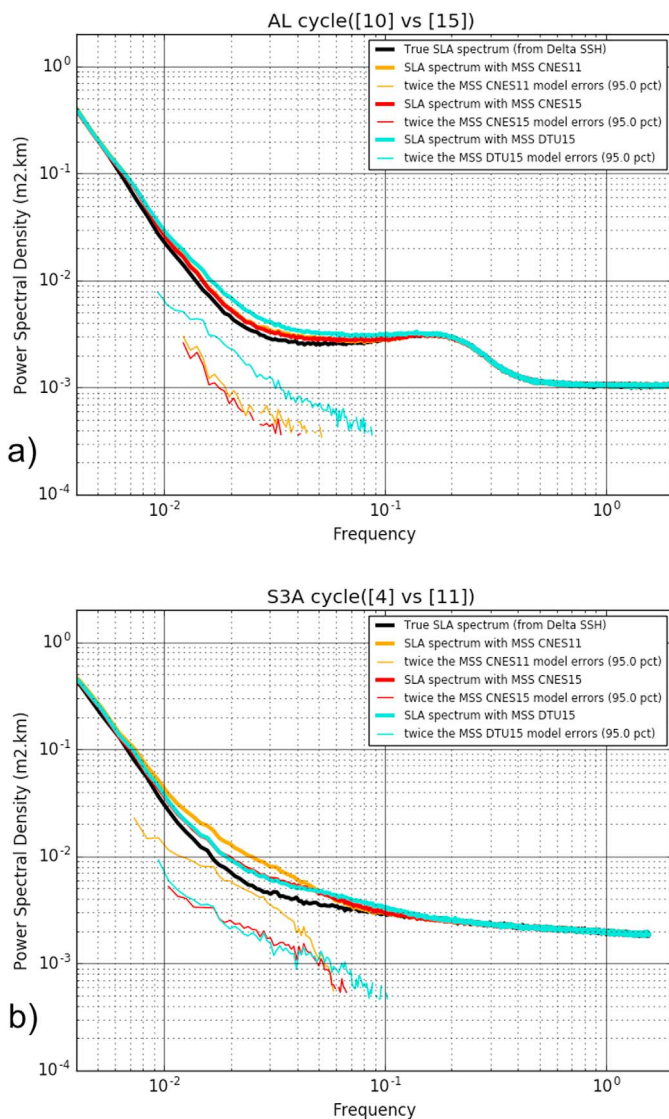


Figure 12. PSD of the true SLA signal+instrumental noise (thick black line), SLA signal including the MSS error (thick color lines), MSS errors (thin color lines) where statistically significant (95% confidence threshold). SLA computed using MSS CNES_CLS11 (yellow lines), MSS CNES_CLS15 (red lines) and MSS DTU15 (blue lines); (a) along SARAL/AltiKa and (b) Sentinel-3A tracks.

it has 6 to 10 times less energy than the so-called hump-error of AltiKa (i.e., the white noise of 1 Hz products; Dibarboore et al. (2014). But it remains significant as it represents 12.1% (CNES_CLS15) to 14.1% (CNES_CLS11) of the SLA signal variance for these wavelengths (Table 5).

5. Absolute Error Assessment With a Focus on the Small Mesoscale

5.1. Error along Charted Tracks

The spectra from previous sections were based on 1 Hz data and made it possible to measure the relative improvements between MSS models. In this section, we use new independent data from Sentinel-3 to compute the absolute MSS error spectra and variance for the wavelengths discussed in section 4. But the Sentinel-3 altimeter is operated in delay-Doppler or synthetic aperture radar mode (also known as SARM), and current SARM products exhibit a red-colored noise floor from 600 m to 50 km. It is necessary to use the full 20 Hz (respectively, 40 Hz) resolution of Sentinel-3 (r respectively, AltiKa).

The methodology is detailed in Appendix A. In essence, by using the difference between SLAs of the same tracks separated by many months, one can infer the true SLA PSD using the difference, because both SLAs are decorrelated and the MSS errors cancel one another out. It then becomes possible to disentangle the PSD of the absolute MSS error itself.

The thick colored lines of Figure 12 show the PSD of the measured SLA (i.e., including the MSS error) using the three MSS models. Using the difference between the SLAs of two cycles separated by 90 days, one can infer the thick black line which is the true PSD of the SLA signal plus the instrumental noise (no more MSS error). The MSS error is stationary, and it has been canceled out in the difference before the black PSD is computed.

Lastly, from the difference between the thick colored lines and the black line of Figure 12, one can infer the thin colored lines which show the PSD of the MSS error for the three models. These curves are only valid for a small range of wavelengths where the difference between two PSDs is statistically relevant (typically from 10–20 to 100–150 km). For longer wavelengths, the ocean dynamics dominate and hide the MSS error, and for shorter wavelengths, the instrument noise dominates and makes it impossible to gauge the MSS error.

Figure 12a focuses on AltiKa when it is operated exactly along the ERS/ENVISAT historical track. We can use it to infer the absolute MSS error along a charted track. For both CNES_CLS models, the error is the same: as expected, the 2011 model was already extremely good on charted tracks, and the improvement with the 2015 version is measurable but very small. The absolute MSS error is also quite small:

These are primarily commission errors: discrepancy between ERS-1, ERS-2, ENVISAT, and AltiKA instruments and processing or corrections, cross-calibration errors with the TOPEX/Jason reference series, smoothing of the mean profile in the 2-D mapping process of the gridded MSS model, etc. Note that this error is consistent with the indirect estimates of Dibarboore et al. (2012) but it provides the first absolute measurement of the MSS errors as well as a wavelength breakdown of this error.

The geographical distribution of the errors is given in Figure 13. The errors observed along AltiKa tracks (Figure 13a) are likely related to

Table 5

Mean Global MSS Error Estimation for Wavelengths Ranging From 30 to 100 km, Expressed in cm (**Bold**) and Percents of the SLA Signal Variance (Parentheses)

	SARAL/AltiKa	Sentinel-3A
CNES_CLS11	0.37 (14.1)	0.84 (70.7)
CNES_CLS15	0.35 (12.1)	0.55 (30.3)
DTU15	0.54 (29.8)	0.55 (30.3)

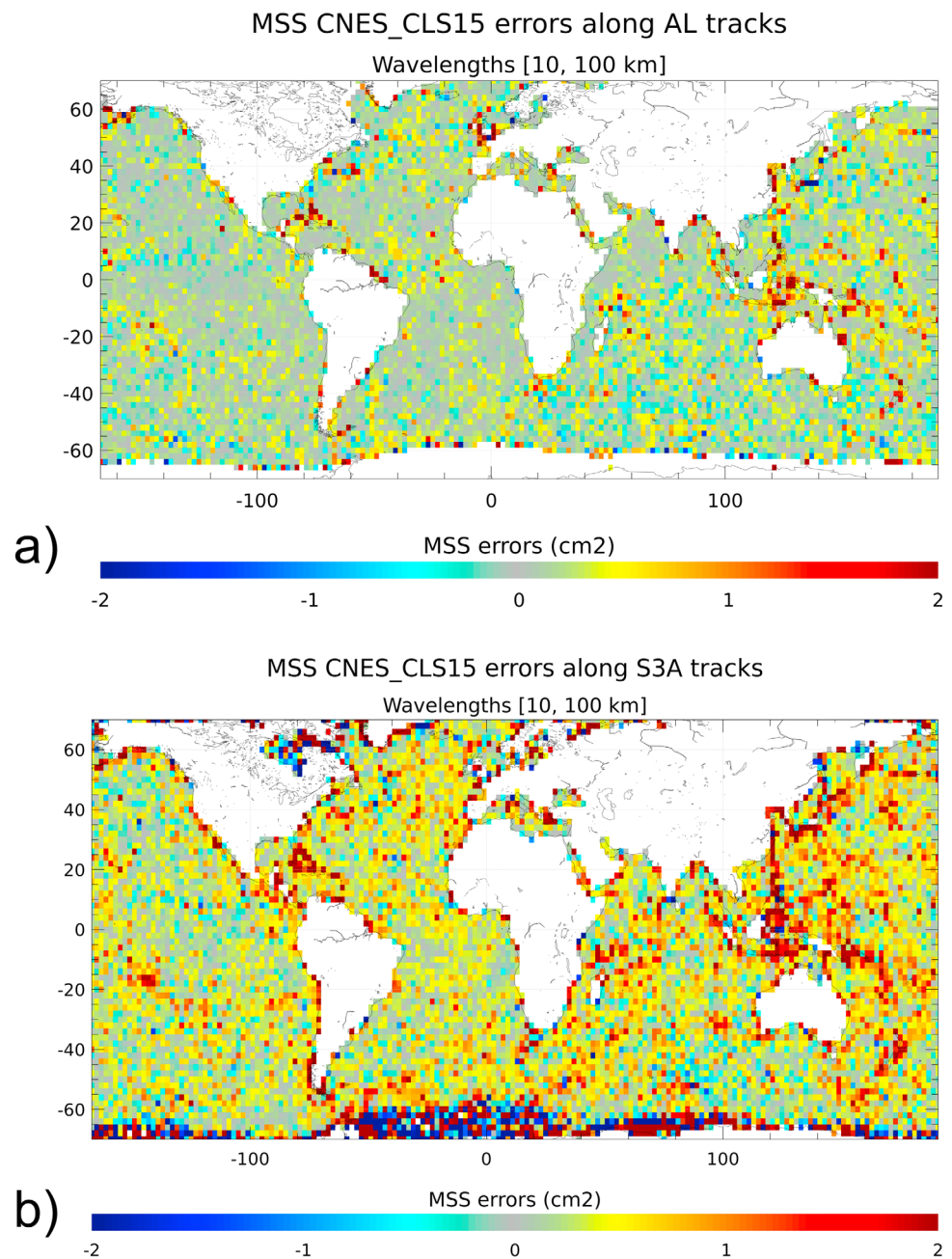


Figure 13. Variance of the absolute MSS errors estimated for MSS CNES_CLS15 for wavelengths ranging from 10 to 100 km (a) along AltiKa and (b) Sentinel-3A tracks.

bathymetric structures that are still incorrectly mapped in current MSS models (smoothing of the ERS/ENVISAT mean profile) and coastal areas that remain poorly represented in the gridded MSS (mean error derived from SSH imperfections in older ERS records). The error can locally reach up to 2 cm^2 , but it is generally only a few mm RMS.

For the DTU15 model, Figure 12a shows that the cyan PSD is 2.5 times greater than the PSD of the CNES_CLS models. This is consistent with the observations from previous sections where the DTU15 was shown to be less precise along charted tracks.

The geographical distribution of the additional DTU15 errors (Figure 14a) shows that most of the errors along charted tracks are located along geodetic features and mesoscale-active regions. This might indicate that:

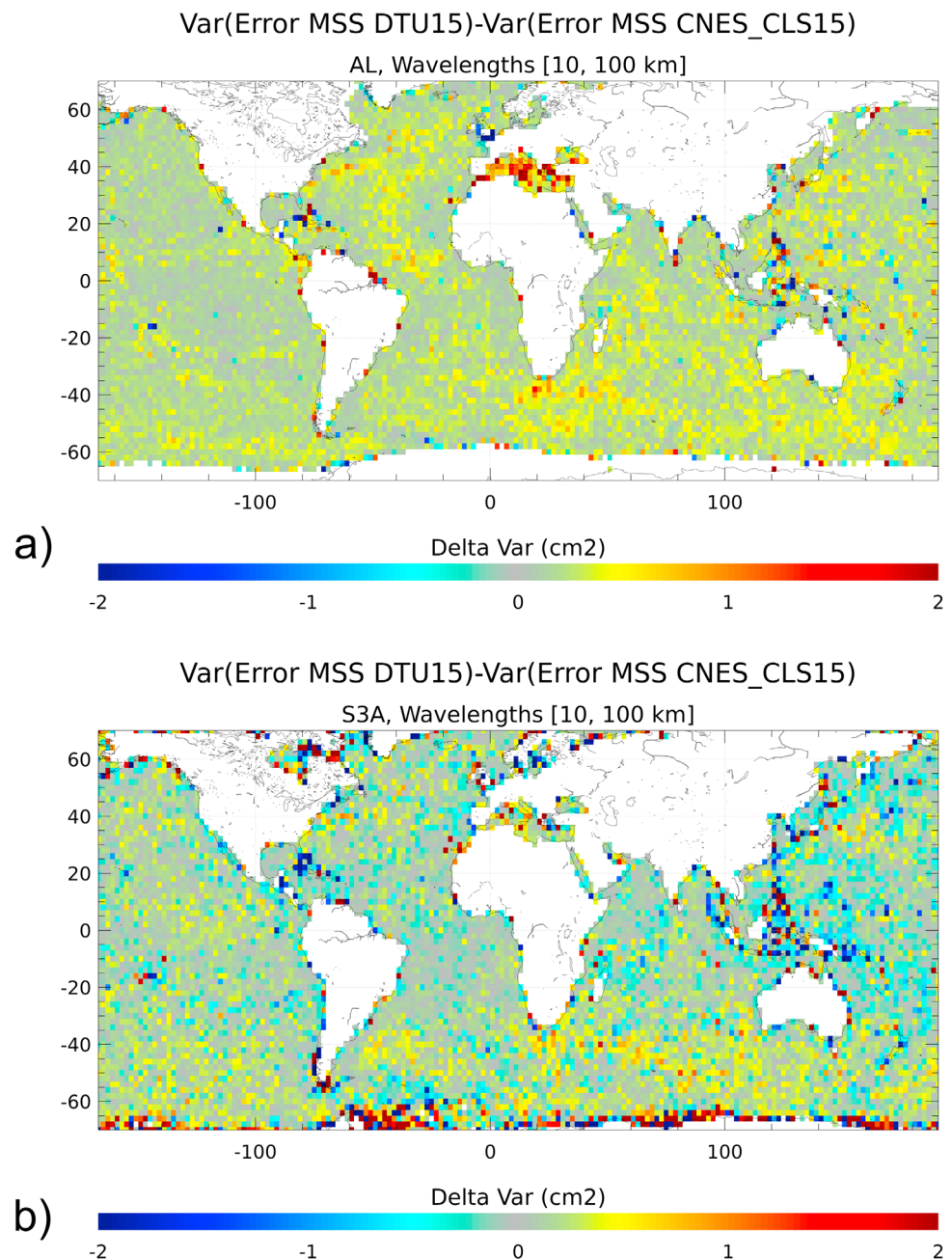


Figure 14. Differences between the variance of the errors estimated for MSS DTU15 and MSS CNES_CLS15 for wavelength ranging from 10 to 100 km (a) along SARAL/AltiKa and (b) Sentinel-3A tracks. Positive value means that errors on MSS CNES_CLS15 are lower than the one observed on MSS DTU15.

1. A fraction of the short wavelength MSS signal is missing in DTU15 because of a higher level of smoothing than in the CNES_CLS models, where the mean profile of ERS/ENVISAT provides more relevant small-scale content along charted tracks.
2. The rest of the DTU MSS error along charted tracks originates in leakage from mesoscale variability (see sections 4.1 and 4.2).

Incidentally, the PSD of the DTU15 error shown in Figure 12a is also clearly linear, with a slope of the order of K-1.5. We speculate that the linear nature of the MSS error PSD is likely related to a geophysical feature: either the omission error of actual geodetic structures in the DTU model, or the leakage from oceanic variability, or a combination of both effects.

5.2. Error Along Uncharted Tracks

Using the same methodology on Sentinel-3 products, we can infer the PSD and geographical distribution of the absolute MSS error.

For CNES_CLS models, there are major differences between AltiKa (charted) and Sentinel-3 (uncharted) data. The errors estimated for CNES_CLS11 along Sentinel-3 tracks account for 70% of the SLA variance (Table 5 and Figure 12), i.e., 5 times more than along AltiKa tracks.

The errors estimated for the CNES_CLS15 model are still substantial as they account for more than 30% of the SLA variance along Sentinel-3 tracks (Table 5 and Figure 12). Although the MSS errors are much slighter compared to the previous MSS version (error reduction by a factor of 2.3), there are still 2.5 times more than along AltiKa tracks, and of the same order of magnitude as the altimeter noise floor.

Figure 13b shows the spatial distribution of the errors measured along Sentinel-3A tracks with the CNES_CLS15 model. They have a clear signature over complex gravimetric structures, in the Indonesian area, and along coastal areas. This map is very consistent with Figure 4a, i.e., the relative improvement from the 2011 model to the 2015 model. The error has essentially the same distribution with less amplitude. This might indicate that the bulk of the error from the CNES_CLS15 model along uncharted tracks originates in omission errors: a larger and denser geodetic data set is still required to further improve the effective resolution of the MSS model.

In contrast, the errors observed for DTU15 MSS along Sentinel-3A tracks are not very different from the charted track of AltiKa (Table 5 and Figure 12). This is consistent with the findings from previous sections: the DTU15 may be smoothed excessively along charted tracks but the result is consistent with the resolution that is accessible away from charted tracks.

The DTU15 error represents approximately 30% of the SLA variance for wavelengths ranging from 30 to 100 km (Table 5), and the PSD of Figure 12b shows as good consistency with the CNES_CLS15 model, except below 20 km where the DTU15 error might be higher.

Incidentally, the error PSD of both 2015 models for Sentinel-3 is clearly linear with a slope of the order of K-1, i.e., less than along charted tracks or the 2011 model. We speculate that the slope difference is the result of a different combination of omission and commission errors:

1. The MSS omission error is higher because these tracks have not been repeatedly sampled for 20 years.
2. But along uncharted tracks, it is also impossible to disentangle small mesoscale, submesoscale or unbalanced motions from true MSS features (as opposed to a 20 year mean profile from ERS-1 to AltiKa where the ocean variability averages out). As a result the commission error from oceanic variability is also higher.

Although the DTU15 model exhibits an error of the same order as the CNES_CLS15 model in terms of variance and PSD, the geographical distribution is not exactly the same (Figure 14b). The spatial distribution of the differences between the MSS errors observed for CNES_CLS15 and DTU15 is similar to the geographic distribution observed along HY-2A tracks at 1 Hz (Figure 4b), with a smaller amplitude because the wavelength band is thinner. The DTU15 errors are slightly larger in mesoscale-active regions (e.g., the Gulf Stream, the Kuroshio, and the Agulhas Current) and they are slightly smaller over specific gravimetric structures and the Indonesian area.

6. Summary and Conclusions

In this paper, we analyzed the errors of different MSS solutions, mainly focusing on wavelengths shorter than 200 km. The CNES_CLS11, CNES_CLS15, and DTU15 MSS models were compared.

Two kinds of MSS model errors were highlighted and quantified. The first is an omission error at the smaller scales of the MSS. This error is essentially driven by the cross-track resolution of gridded geodetic altimetry data and by how much smoothing is performed when the along-track altimetry profiles are regredded into a 2-D model.

The omission errors are usually small along the ground tracks of a repeat orbit, while they can explain most of the MSS errors away from charted tracks. Omission errors are the main source of error of the 2011 model, which did not benefit from the very dense and trustworthy data sets collected by geodetic altimeters and

used for the 2015 MSS models. Thanks to this additional coverage, the omission error of recent models was reduced by a factor of 2.3 for wavelengths ranging from 30 to 100 km. Moreover, thanks to the high inclination of Cryosat-2 and its good coastal coverage, omission errors were significantly reduced: there was a gain of more than 22% of SLA variance in coastal areas and locally more than 20 cm² at high latitudes.

Thanks to the substantial reduction in omission errors, the MSS errors are now more geographically homogeneous. Indeed, when AltiKa drifted away from its historical ERS/ENVISAT ground track, the SLA error increased by 0.42 cm RMS per km with the 2011 MSS model, whereas this value decreases to 0.30 cm RMS per km or less with 2015 models.

The second type of error is commission errors. These are essentially linked to how altimetry errors and dynamic ocean variability are isolated from the true MSS content. Because the separation is not perfect, ocean dynamics and geophysical errors may leak into the MSS model and in turn degrade the quality of SLA products based on the said MSS model. In the open ocean, mesoscale variability dominates commission errors, while altimetry errors dominate in coastal regions (e.g., imperfect tidal correction of the SSH).

Commission errors are naturally mitigated when long time series on repetitive orbits (e.g., TOPEX or ERS tracks) are used to generate a so-called mean profile, i.e., a local one-dimensional MSS along the altimeter track. In contrast, the problem is more complex for geodetic altimeters because their dense geographical coverage implies that the revisit time very long (e.g., 6–12 months). The risk of seeing oceanic variability leak into MSS models can be mitigated at the larger mesoscale with the use of external data sets (e.g., DUACS maps), but it is much more challenging to mitigate the dynamic signal at wavelengths shorter than 200 km or in the regions that are not covered by external data sets (e.g., sea ice).

A significant fraction of the large-scale MSS model differences observed at high latitudes was shown to originate in different ocean variability corrections or altimeter cross-calibration methods in the MSS CNES_CLS15 and DTU15. For the global ocean, SLA based on the CNES_CLS15 model exhibit a variance reduction of approximately 2.4 cm RMS in comparison with the DTU15, whereas in the Arctic ocean, the variance reduction is only 0.6 cm RMS.

With the CNES_CLS15 MSS model, the leakage of oceanic variability at wavelengths shorter than ~200 km is shown to be of the order of 1 cm², i.e., 9.3% of the variance observed along Jason-2 tracks. For the DTU15 model, the leakage is almost twice as high, with 1.9 cm² (17%).

When comparing 2011 and 2015 MSS models, we observe a shift of the relative weight of these two sources of error. Omission errors have been reduced with the use of additional geodetic altimeter measurements. But in turn the new geodetic data sets have introduced commission errors in the 2015 models. Because the commission errors are substantially smaller, the net result is a dramatic improvement in the newer MSS models (absolute error reduced by a factor of 2.3).

Still, for wavelengths shorter than 100 km, the residual errors of recent models represent nearly 30% of the SLA variance along uncharted Sentinel-3 tracks. This is twice as much as for a charted track that benefits from a 20 year mean profile. This error is also of the same order of magnitude as the instrumental noise floor of Sentinel-3. It is therefore a limiting factor for fully exploiting altimetry measurement for wavelengths shorter than 100 km.

In other words, reducing the error of MSS models along uncharted tracks remains a critical improvement needed to benefit fully from new and upcoming altimeter technology (e.g., Jason-CS/Sentinel-6 or SWOT, SWOT, 2016) and improved data processing (e.g., noise measurement reduction techniques, Zaron & DeCarvalho, 2015) and retracking (e.g., Garcia et al., 2014), which are expected to reduce the instrument noise floor by a factor of 2–5 compared to a Jason-class altimeter.

In addition to data reprocessing and better MSS algorithms, a critical way forward for improving future MSS models is to keep collecting geodetic altimeter data at the highest possible resolution in the along-track and cross-track directions. Because Cryosat-2 has a fixed 1 year cycle (i.e., 8 km cross-track resolution), it is essential to collect data sets from other altimeters to reduce the number of omission errors. This is currently possible as HY-2A is now in a geodetic phase, AltiKa is on a drifting orbit, and Jason-2 is on a so-called long-repeat orbit.

Lastly, it is also essential to collect very long time series of geodetic measurements to better average out ocean variability leakages at scales that are not resolved with DUACS maps. For this purpose, it would be

extremely beneficial to operate the current geodetic altimeters for as long as possible, and to consider adding future ageing missions on a geodetic orbit (e.g., Jason-3 when Jason-CS/Sentinel-6 is commissioned, or Sentinel-3A/3B in the future).

Appendix A: A New Approach for MSS Error Characterization at the Small/Submesoscale

The methodology used to quantify MSS errors is based on an analysis of the SLA signal considered over two different cycles, noted A and B.

We note H_i the SLA measured along a repetitive track during a cycle i . It is obtained as the difference between the altimeter SSH measurement and the MSS. If the MSS model is not perfect, it can be broken down into the true content (MSS_{true}) and a constant error (e):

$$H_i = \text{SSH}_i - \text{MSS} = \text{SSH}_i - \text{MSS}_{true} - e = H_{true,i} - e$$

Moreover, the true SLA can also be broken down into a random component (h_i) and a periodic component, such as unbalanced motions forced by stationary internal tides (w_i):

$$H_i = h_i - e + w_i$$

Using the sum and difference of H_A and H_B for two cycles A and B we obtain the following equation:

$$\begin{aligned} & V(H_A - H_B) - V(H_A + H_B) = \\ & 4V(e) + 4C(w_A, w_B) - 4C(e, w_B) - 4C(e, w_A) + 4C(h_A, w_B) + 4C(h_B, w_A) \end{aligned} \quad (1)$$

where V and C are, respectively, the variance and covariance functions.

To separate and quantify these terms, we make three approximations:

1. The SLA signal is completely uncorrelated between the two cycles A and B. So the cycles A and B are selected to be as far from one another as possible to ensure a good decorrelation of h_A and h_B , at least for wavelengths shorter than 200 km.
2. Because we use independent data sets and a different time period, there is no covariance between the SLA signal and the MSS errors.
3. The MSS error is constant, i.e., the same for all cycles. This is not strictly true because the satellite ground track moves from cycle to cycle, but the approximation is justified here because we selected satellites and periods when the orbit is properly maintained (within 1 km).

Lastly, to isolate w from h and e , we make the following assumptions:

1. The covariance between the SLA signal h_i and the internal tide signal w_j , as well as the covariance between w_A and w_B , can be minimized by properly selecting cycles A and B based on the orbit aliasing properties for the main tidal constituents. Considering the main wave component M2, a separation of 5 cycles for AltiKa leads to a $\sim\pi/2$ phasing of the M2 tide. For Sentinel-3A, 4, and 7 cycles are necessary (respectively, $\sim-\pi/2$ and $\pi/2$ phasing). This selection is however not optimized for the third wave component N2, leading to a nearly perfect phasing for AltiKa and a nearly 2π (4 cycles delta) or π (7 cycles delta) phasing for Sentinel-3. Although not perfect, this selection of cycles helps mitigate the influence of coherent internal tides in our analysis.
2. The covariance between the MSS error e and the internal wave signal w_i is negligible. Indeed, MSS computation is based on the merging of measurements from different altimeters, which minimizes the influence of stationary internal tides in the MSS models.

Equation (1) can then be approximated to give equation (2):

$$V(H_A - H_B) - V(H_A + H_B) \approx 4V(e) \quad (2)$$

Using the sum of and difference between the SLAs from two well-chosen cycles and independent data, it is possible to extract the absolute error of the MSS model.

Appendix B: MSS Commission Errors and SLA Variance

Using the notations from Appendix A, the variance of H_i is given by the following equation:

$$V(H_i) = V(h_i) + V(e) - 2C(e, h_i) \quad (3)$$

When e is independent of h_i , the covariance between these two components is zero and $V(H_i)$ is larger than the variance of the true signal, due to the $V(e)$ contribution. In otherwords, if the MSS error is not zero and not correlated with the instantaneous SLA content, the SLA variance increases.

Conversely, when these two components are correlated, $V(H_i)$ is smaller than $V(h_i)$ because of $C(e, h_i)$. This occurs when a fraction of the ocean dynamic variability leaks into the MSS model.

Acknowledgments

The generation of the CNES_CLS15 MSS model and the error analysis of the different MSS models were funded by CNES in the framework of the SWOT and SALP projects. The CNES_CLS15 MSS model is available on Aviso+ (<https://www.aviso.altimetry.fr/en/data/products/auxiliary-products/mss.html>).

References

- Andersen, O. B., Knudsen, P., & Stenseng, L. (2015). The DTU13 MSS (Mean Sea Surface) and MDT (Mean Dynamic Topography) from 20 years of satellite altimetry. In S. Jin & R. Barzaghi (Eds.), *International Association of Geodesy Symposia* (IGFS 2014, Vol. 144, pp. 1–10). Cham, Switzerland: Springer. https://doi.org/10.1007/1345_2015_182
- Boy, F., Desjonquères, J. D., Picot, N., Moreau, T., & Raynal, M. (2017). CryoSat-2 SAR-Mode over oceans: Processing methods, global assessment, and benefits. *IEEE Transactions on Geoscience and Remote Sensing*, 55(1), 148–158. <https://doi.org/10.1109/TGRS.2016.2601958>
- Bretherton, F. P., Davis, R. E., & Fandry, C. B. (1976). A technique for objective analysis and design of oceanographic experiments applied to MODE-73. *Deep Sea Research and Oceanographic Abstracts*, 23, 559–582.
- Chelton, D. B., Schlax, M. G., & Samelson, R. M. (2011). Global observations of nonlinear mesoscale eddies. *Progress in Oceanography*, 91, 167–216. <https://doi.org/10.1016/j.pocean.2011.01.002>
- Dibarboire, G., Boy, F., Desjonquieres, J. D., Labroue, S., Lasne, Y., Picot, N., et al. (2014). Investigating short-wavelength correlated errors on low-resolution mode altimetry. *Journal of Atmospheric and Oceanic Technology*, 31, 1337–1362. <https://doi.org/10.1175/JTECH-D-13-0081.1>
- Dibarboire, G., Renaudie, C., Pujol, M.-I., Labroue, S., & Picot, N. (2011). A demonstration of the potential of CryoSat-2 to contribute to mesoscale observation. *Advances in Space Research*, 50, 1046–1061. <https://doi.org/10.1016/j.asr.2011.07.002>
- Dibarboire, G., Schaeffer, P., Escudier, P., Pujol, M.-I., Legeais, J. F., Faugère, Y., et al. (2012). Finding desirable orbit options for the “Extension of Life” phase of Jason-1. *Marine Geodesy*, 35, 363–399. <https://doi.org/10.1080/01490419.2012.717854>
- Dufau, C., Orstynowicz, M., Dibarboire, G., Morrow, R., & La Traon, P.-Y. (2016). Mesoscale resolution capability of altimetry: Present & future. *Journal of Geophysical Research*, 121, 4910–4927. <https://doi.org/10.1002/2015JC010904>
- Escudier, P., Couhert, A., Mercier, F., Mallet, A., Thibaut, P., Tran, N., et al. (2018). Satellite radar altimetry: Principle, accuracy & precision. In D. Stammer & A. Cazenave (Eds.), *Satellite altimetry over oceans and land surfaces* (Chapter 1). Boca Raton, FL: Taylor and Francis. <https://www.routledge.com/Satellite-Altimetry-Over-Oceans-and-Land-Surfaces/Stammer-Cazenave/p/book/9781498743457>
- Garcia, E. S., Sandwell, D. T., & Smith Walter, H. F. (2014). Retracking CryoSat-2, Envisat and Jason-1 radar altimetry waveforms for improved gravity field recovery. *Geophysical Journal International*, 196, 1402–1422.
- Hernandez, F., & Schaeffer, P. (2000). *Altimetric mean sea surfaces and gravity anomaly maps inter-comparisons AVISO* (Tech.R ep. AVI-NT-OII-5242-CLS). Toulouse, France: Cent. Natl. d'Etudes Spatiales.
- Hernandez, F., & Schaeffer, P. (2001). *Surface moyenne océanique: Support scientifique à la mission altimétrique Jason?1, et à une mission micro-satellite altimétrique* (Rapp. CLS/DOS/NT/00.341). Ramonville Saint-Agne, France: Collect. Localisation Satell.
- Jiang, X., Lin, M., Liu, J., Zhang, Y., Xie, X., Peng, H., et al. (2012). The HY-2 satellite and its preliminary assessment. *International Journal of Digital Earth*, 5(3), 266–281.
- Le Traon, P.-Y., Bonekamp, H., Antoine, D., Bentamy, A., Breivik, L. A., Chapron, B., et al. (2014). Use of satellite observations for operational oceanography: Recent achievements and future prospects. *Journal of Operational Oceanography*, 8(Suppl 1), s12–s27.
- Le Traon, P.-Y., & Ogor, F. (1998). ERS-1/2 orbit improvement using TOPEX/POSEIDON: The 2 cm challenge. *Journal of Geophysical Research*, 103, 8045–8057.
- Picot, N., Lachiver, J. M., Lambin, J., Poisson, J. C., Legeais, J. F., Vernier, A., et al. (2013). Towards an operational use of HY-2A in SSALTO/DUACS: Evaluation of the altimeter performances using S-IGDR data from NSOAS. Presented at the 2013 Ocean Surface Topography Science Team meeting (Boulder, USA). Study sponsored by CNES (Toulouse, France) in the frame of their collaboration with CNSA.
- Pujol, M.-I., Faugère, Y., Taburet, G., Dupuy, S., Pelloquin, C., Ablain, M., et al. (2016). DUACS DT2014: The new multi-mission altimeter data set reprocessed over 20 years. *Ocean Science*, 12, 1067–1090. <https://doi.org/10.5194/os-12-1067-2016>
- Schaeffer, P., Faugere, Y., Legeais, J. F., Ollivier, A., Guinle, T., & Picot, N. (2012). The CNES CLS11 global mean sea surface computed from 16 years of satellite altimeter data. *Marine Geodesy*, 35, 3–19.
- SWOT (2016). *Surface water and ocean topography mission (SWOT\$) Project Science Requirements Document. RevA release (E. Rodriguez, Document Custodian)*. California, CA: Jet Propulsion Laboratory. Retrieved from https://swot.jpl.nasa.gov/docs/D-61923_SRD_Rev_A_20160318.pdf, last accessed 13 June 2018
- Tarantola, A., & Valette, B. (1982). Generalized nonlinear inverse problems solved using the least square criterion. *Reviews of Geophysics*, 20, 219–233.
- Valladeau, G., Thibaut, P., Picard, B., Poisson, J. C., Tran, N., Picot, N., et al. (2015). Using SARAL/AltiKa to improve Ka-band altimeter measurements for coastal zones, hydrology and ice: The PEACHI prototype. *Marine Geodesy*, 38(Suppl. 1), 124–142.
- Zanife, O. Z., Vincent, P., Amarouche, L., Dumont, J. P., Thibaut, P., & Labroue, S. (2003). Comparison of the Ku-Band range noise level and the relative sea-state bias of the Jason-1, TOPEX, and Poseidon-1 radar altimeters. *Marine Geodesy*, 26, 201–238.
- Zaron, E., & DeCarvalho, R. (2015). Identification and reduction of retracker-related noise in altimeter-derived sea-surface height measurements. *Journal of Atmospheric and Oceanic Technology*, <https://doi.org/10.1175/JTECH-D-15-0164>